Master Thesis
TVVR 20/5001

Design of RCC gravity dam and FEM modelling in GeoStudio – Longtan dam

Eugenia Correa Saracco
Patrick Lucas Bochnak

Division of Water Resources Engineering
Department of Building and Environmental Technology
Lund University

Design of RCC gravity dam and FEM modelling in GeoStudio Longtan dam

By:
Eugenia Correa Saracco
Patrick Lucas Bochnak

Master Thesis

Division of Water Resources Engineering
Department of Building & Environmental Technology
Lund University
Box 118
221 00 Lund, Sweden

Water Resources Engineering
TVVR-20/5001
ISSN 1101-9824

Lund 2020
www.tvrl.lth.se

Master Thesis
Division of Water Resources Engineering
Department of Building & Environmental Technology
Lund University

English title:	Design of RCC gravity dam and FE-modelling in GeoStudio – Longtan dam
Author(s):	Eugenia Correa Saracco Patrick Lucas Bochnak
Supervisor:	Magnus Larson
Examiner:	Rolf Larsson
Language	English
Year:	2020
Keywords:	RCC; China; Longtan dam; Flood routing; GeoStudio

Acknowledgements

This master's degree project was carried out at the Division of Water Resources Engineering, Faculty of Engineering (LTH) at Lund University. This work was performed in collaboration with Vattenfall, Energiforsk and Hohai University in Nanjing, China during the spring of 2019.

We would like to express our sincerest gratitude to our supervisor Professor Magnus Larson at the Division of Water Resources Engineering, Lund University for his valuable critics and guidance throughout the project. We would also like to thank Professor Dai and his student Li Yao for their help during our stay in China. Finally, we would like to thank James Yang at both Vattenfall and Energiforsk for giving us the opportunity to participate in this project, and for serving as a bridge between Lund University and Hohai University.

Eugenia Correa Saracco and Patrick Lucas Bochnak
Lund, February 2020

Abstract

China's rapid economic development has led to a continuously increasing energy demand and the country is the world's biggest energy user as of today. The country accounts for around 23% of the global energy production, but 70% of the Chinese energy is generated with coal power and China is the biggest emitter of CO_2 in the world. The Chinese government has set a couple of goals to reduce the country's carbon emissions and to increase the share of renewable energy. Hydropower is a renewable energy source and the construction of large dams will likely be one of the strategies to meet the rising energy demand in a more sustainable way. The failure of dams can be devastating, and it is therefore important that they are designed with proper safety measures. In this report, the Longtan dam has been used as a reference to conduct a preliminary design of a large gravity dam and to evaluate its safety. The preliminary design was based on dam site data provided by the College of Water Conservancy and Hydropower Engineering at Hohai University in Nanjing, China. The structural analysis of the dam was conducted with both analytical and numerical methods. The analytical calculations showed that the dam is safe against overturning, but that there is risk for a sliding failure. The analytical stress analysis showed that the stresses in the dam do not exceed the material capacity. The numerical analysis was done in the commercial FEM software suite GeoStudio. The results from the seepage analysis showed that the peak seepage velocities in the foundation are $4{,}5\text{-}5{,}0 \cdot 10^{-7}$ m/s, and that it is unlikely that the seepage will compromise the structural integrity of the dam. The numerical stress analysis revealed that the stresses are 0-2 MPa in most of the dam body, but that the dam toe is subjected up to 12 MPa compression and that the dam heel is subjected up to 16 MPa tension. This indicates that a tensile failure will occur in the dam heel, which will lead to cracks in the concrete and a redistribution of the stresses. It is therefore advised that the dam heel is reinforced to avoid potential problems with seepage.

Table of contents

1. Introduction

Description of the background, aim and objectives of the project, as well as its scope and limitations. An outline of the report is provided at the end of the present chapter.

1.1. Background

1.1.1. Hydropower in China

China is the country that generates the most hydropower in the world, and there are around 88 000 dams of various sizes in China (Liu et al., 2013). The country had an installed hydropower capacity of 352 GW as of 2018, which is equal to a quarter of the world's total hydropower capacity and 18,5% of China's total electric power capacity (International Hydropower Association, 2019).

But China needs to utilize more renewable energy resources if the country wants to meet its continuously growing energy demand in a more sustainable way. In 2014, China stood for 23% of the global energy production while it also became the largest energy consumer in the world. Around 70% of the country's energy is produced with coal power, and China is the largest CO_2 emitter in the world since 2015.

The Chinese government has set a couple of goals to tackle this problem. The government wants non-fossil fuel to account for 15% of the energy supply by 2020, and to reduce the country's CO_2 emissions with 40-45% in 2020 as compared to the 2005 levels (Zhang et al., 2017). Another goal is to make renewable energy resources cover 35% of the country's energy consumption by 2030 (Shen, 2018).

Hydropower is a renewable energy resource and it is estimated that there is a theoretical possibility to generate 694 GW from hydropower in China, which makes China the richest country in the world in terms of potential hydropower resources (Huang and Yan, 2009). China has plans to expand its hydropower capacity to 430 GW by 2020 (Lai and Warner, 2016). Moreover, in 2030

further development of hydropower will be made at the Jinsha River, Yalong River, Nu River and the Yarlung Zangbo River (Zhang et al., 2019).

1.1.2. Construction of dams in China

Dams and embankments have been constructed in China for thousands of years for irrigation and flood control purposes. The remains of the oldest ancient structures are over 2 600 years old and there are systems that are still active today that are over 2 000 years old (Wang et al., 2014). The Dujiangyan irrigation system, the oldest operating irrigation and flood control system in China, is more than 2 200 years old (Zhang, 1999), (UNESCO, n.d). The Dujiangyan irrigation system can be seen in figure 1.

Figure 1. The Dujiangyan irrigation system (Ancient Origins, 2013)

However, the first modern and advanced dams in China were constructed with foreign technology during the first half of the 20th century. Before 1949, there were 22 large dams that had been constructed in the country (Zhang, 1999). The first hydropower station that was built in China is the Shilong dam near Kunming, Yunnan province. It was finished in 1910 and it is still in service today (Li et al., 2018).

Between 1950 and 1957 large dams in China were mainly constructed with the purpose of controlling large floods in rivers like the Huai, Han and Huang. The dams that were built during this time period usually have a height of 50-150 meters. One of the dams from this era is the 106-meter-high Sanmenxia dam

in Hunan province (Wang et al., 2014). The establishment of the Sanmenxia hydropower station is historically important because the project is regarded as the starting point of China's continuous and scientific development of hydropower in the country (Li et al., 2018). The Sanmenxia hydropower station can be seen in figure 2.

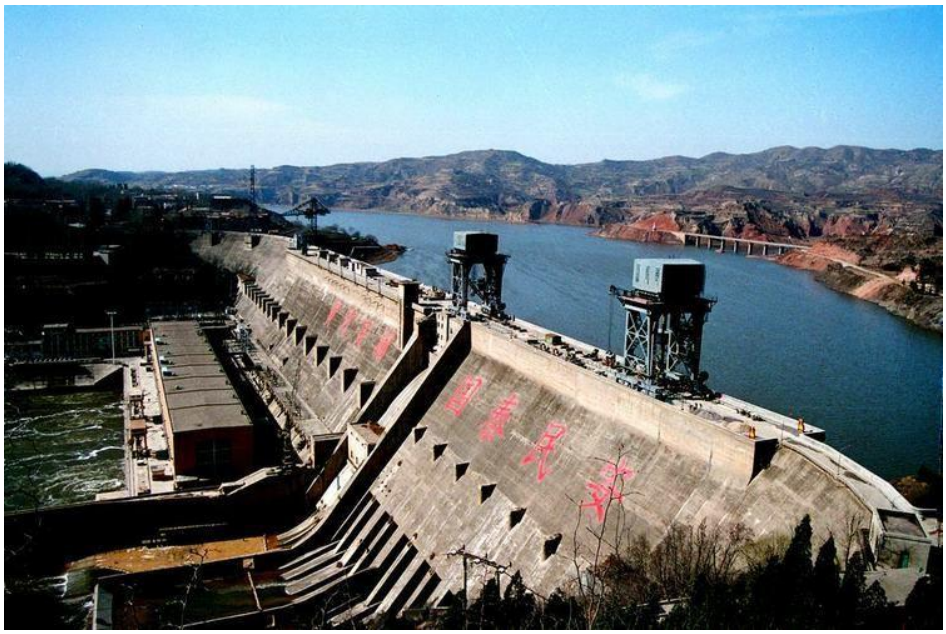

Figure 2. Sanmenxia dam (Alchetron, 2018)

During 1958 to 1966 China made heavy investments to develop the infrastructure in the country and many large dams were constructed during these years as a subsequent result. One of the dams that was built during this time period is the Liujiaxia dam in Gansu province (Wang et al., 2014). The Liujiaxia power station was the first hydropower station in China with a capacity of 1 GW (Li et al., 2018).

Between 1967 and 1986 the quality of the dams and the construction technology in China was greatly improved. During this time a smaller number of large dams were constructed compared to the years prior, but important projects like the Gezhouba dam on the Yangtze River in Hubei province were launched during this period (Wang et al., 2014). The Gezhouba power station

was the first major project on the Yangtze River and it is the forerunner to the Three Gorges dam (Li et al., 2018), (Wang et al., 2014).

Since 1987, China's rapid economic development has both stimulated the development and construction of large dams as well as it has created a huge demand for electricity in the country (Wang et al., 2014). Some examples of the dams that have been built in China in the past 30 years are the Longtan dam, the Three Gorges dam and the Xiaowan dam. The Three Gorges dam is able to generate up to 22 500 MW and it is the world's largest dam in terms of capacity (Cleveland and Morris 2014). The Three Gorges dam can be seen in figure 3.

Figure 3. The Three Gorges dam by Le Grand Portage (CC BY 2.0)

1.1.3. Consequences of dam construction

The construction of dams comes at the cost of altered and damaged ecosystems. The temperature and the quality of the water is different in a reservoir than in a natural free-flowing river (International Rivers, n.d.). Dams also trap sediment and organic materials in the reservoir (Scientific American, 2018). Furthermore, the water level in a reservoir and the outflow from it is controlled by humans and not by nature. These changes harm the ecosystems both at the dam site and downstream of it. And when upstream areas are being dammed up, species lose their habitats and risk going extinct. Dams are also barriers that prevent migration of fish and the transportation of seeds along the river.

The construction of dams can have social consequences as well. Dam projects can force people into migration, and sustainable communities might be eradicated for the favour of unsustainable cities (Johansson and Sellberg, 2006). There is also a potential health hazard, as reservoirs make good breeding grounds for vector-borne diseases in tropical and subtropical environments (Lerer and Scudder, 1999).

But further construction of large dams can be expected in China and other parts of the world, since the energy demand is growing and hydropower is a renewable energy source. The failure of large dams can have disastrous consequences. It is therefore of interest to study the design process behind these structures and the safety of them.

1.2. Aim and objectives

The main aim of this project is to conduct a preliminary design of a roller compacted gravity dam located in southern China, while increasing the knowledge of large dam structures like the Longtan dam. Furthermore, it must be ensured that the calculated structure complies with the safety regulations and that its performance does not negatively affect the downstream area.

In order to achieve the aim, the following objectives are defined:

- Establish the design flow of the dam.
- Determine the stability of the structure against sliding, overturning and seepage, and ensure that the compressive capacity of the material is not surpassed.
- Determine the stress behaviour of the non-overflow section and ensure that it satisfies the safety requirements with regard to the compressive and tensile capacity of the structural material.
- Identify the most sensitive and vulnerable areas of the design.
- Determine the consequences that the performance of the dam has on downstream erosion.

1.3. Scope and limitations

The present is a preliminary design of a roller-compacted gravity dam, thus, detailed calculations and design of the different components of the dam is excluded. All the assumptions followed in the calculations performed within the present report are the ones inherent in preliminary designs that use the gravity method. These are (Novak et al., 2007):

- The dam's body material (concrete) is homogeneous, isotropic and uniformly elastic.
- All the loads are carried by gravity action of vertical parallel-sided monoliths with no mutual support between adjacent cantilevers.
- No differential movements affecting the dam or foundation occur as a result of the water load from the reservoir.

1.4. Outline

The project is divided into 12 chapters with the following content:

Chapter 1 describes the background, aim and objectives of the report as well as its scope and limitations *(Written by ECS and PLB).*

Chapter 2 provides the project description including information about the Longtan dam and its site location, the methodology followed throughout the project and the software used *(Written by PLB).*

Chapter 3 includes a brief theoretical background of dams, dam safety, spillways and outlets. It also gives an overview of the flood routing calculations, analytical calculations and FEM modelling *(Written by PLB).*

Chapter 4 summarizes the feasibility studies required prior to a dam project *(Written by ECS and PLB).*

Chapter 5 contains flood routing calculations and the resulting design flow *(Written by ECS).*

Chapter 6 presents the design of the non-overflow section of the dam *(Written by ECS).*

Chapter 7 presents the design of the overflow section of the dam *(Written by PLB).*

Chapter 8 describes the loads considered in the calculations *(Written by ECS).*

Chapter 9 describes and presents the application of the partial coefficient method used to obtain the load combination cases *(Written by ECS).*

Chapter 10 contains the analysis of the stability of the structure against overturning, sliding and compression *(Written by ECS)*. It also includes a FE-analysis of the seepage conducted in GeoStudio *(Written by PLB).*

Chapter 11 presents how the gravity method is applied to analyse the stresses in the structure, and assesses the permissible stresses *(Written by ECS)*. It also includes a FE-analysis of the stresses conducted in GeoStudio *(Written by PLB).*

Chapter 12 summarizes the results obtained and offers some final conclusions regarding the preliminary design of the dam obtained and the followed methodology.

2. Project description

General information about the Longtan dam and its site location, the methodology followed throughout the project and the software used.

2.1. Case of study: Longtan dam

The Longtan dam is a roller-compacted concrete (RCC) gravity dam on the Hongshui River in China. It is located 15 kilometres from Tian'e County in the Guangxi Province. When it was finished it was the tallest and the biggest RCC dam in the world (Wang et al., n.d.), (Warren, 2015). Figure 4 shows how the Longtan dam looks like during operation.

The planning of the Longtan dam took circa 40 years. A preliminary design was approved in 1989, but several years were spent to optimize the design with the aim of shortening the construction time and reducing the cost (Qingchung and Feng, n.d.). The construction of the dam began in 2001 and it was officially finished in 2009 (Malcolm Dunstan and Associates, n.da).

Figure 4. The Longtan dam during operation (Malcolm Dunstan and Associates, n.da)

The purpose of the dam is power generation, flood control, and navigation. It is equipped with a ship-lift, nine generators, seven surface spillways, two bottom outlets and a trajectory bucket energy dissipation arrangement (Chinese National Committee on Large Dams, n.d.), (Shurong and Feng, n.d.). Some of the technical specifications of the Longtan dam can be seen in table 1.

Table 1. Technical specifications of Longtan dam (source: Chinese National Committee on Large Dams)

Dam height	216,5 m
Dam length	849,44 m
Upstream slope ratio	1:0,25
Downstream slope ratio at the non-overflow (NOF) section	1:0,73
Downstream slope ratio at the overflow (OF) section	1:0,625
Total installed capacity	6 300 MW
Reservoir capacity	27 270x10^6 m^3
Size of each spillway opening	15x20 m^2
Maximum discharge	27 134 m^3/s

The non-overflow cross section of the dam can be seen in figure 5, and the overflow cross section of the dam can be seen in figure 6. Water from the reservoir can flow over the structure at the overflow section, while not over the non-overflow section.

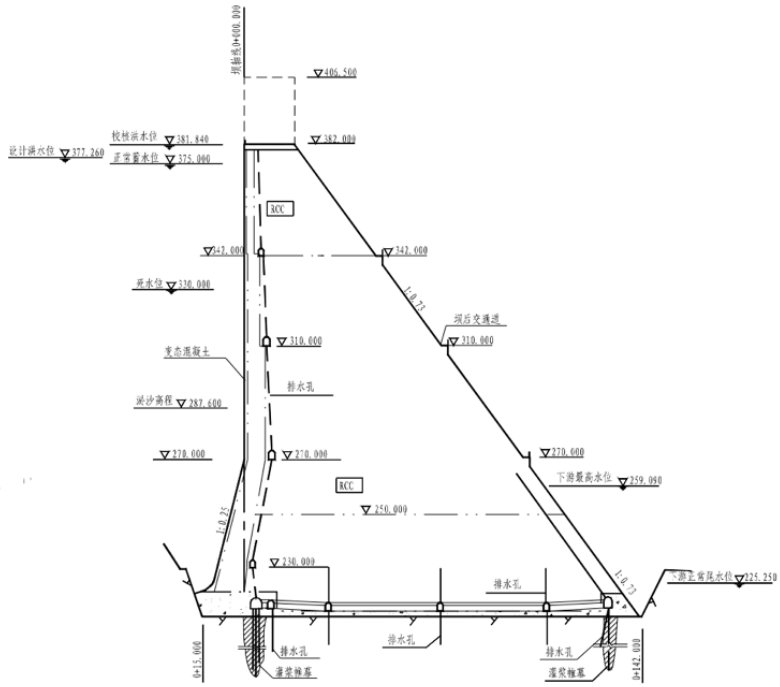

Figure 5. Non-overflow section of the Longtan dam (Chinese National Committee on Large Dams, n.d.)

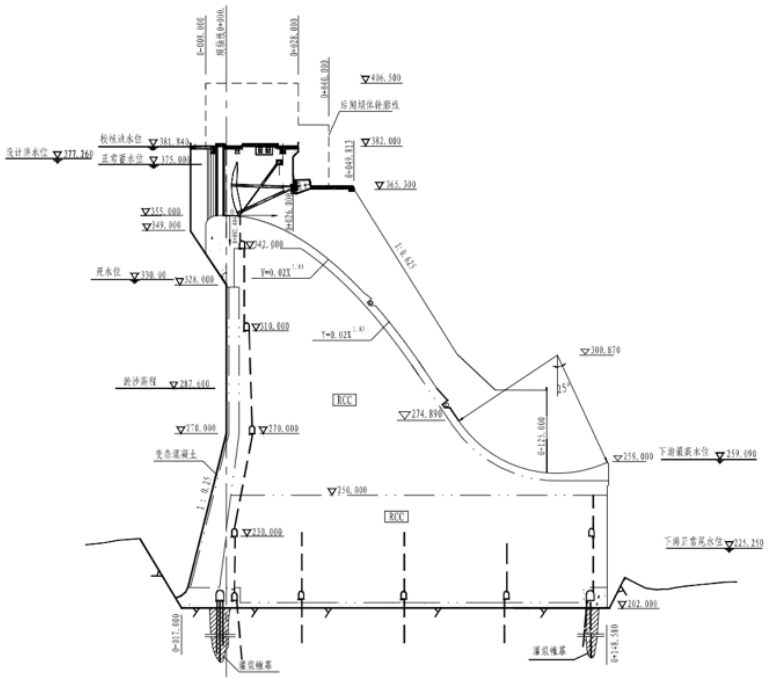

Figure 6. Overflow section of the Longtan dam (Chinese National Committee on Large Dams, n.d.)

2.2. Dam site data

The following section contains data from the site of the Longtan dam provided by the College of Water Conservancy and Hydropower Engineering at Hohai University in Nanjing, China.

2.2.1. Site description

The Longtan dam is located at an elevation of +195 m in a V-shaped valley in the upstream reaches of the Hongshui River. On the left bank side of the valley there is a wide and thick mountain with a smooth profile. On the right bank side there is gully and the landform is not as neat as on the left bank. The length of the Hongshui River is 1 573 km and it is a part of the upper and middle reaches of the Xi River system. The basin area above the dam site is 98 500 km^2, which makes 71% of the whole basin area of the Hongshui River. The basin above the dam site has many large tributaries, with complex terrain.
The dam is situated in a relatively stable location. There are no active faults in the region and there is no background for earthquakes. The only risk for seismic activity in the region is posed by potential peripheral earthquakes.

2.2.2. Strat lithology

The upstream stratum is made up of a thin layer of silicon argillaceous slate and a medium thick layer of siliceous muddy limestone. The stratum at the dam site and downstream contains thick calcium limestone, siltstone and interbedded argillite and is classified as hard to medium hard. The country rock stratum consists of sandstones, or of interbedded stone board made of sandstone or muddy limestone. The country rock stratum possesses a high strength. The dam site rock stratum is of monocline structure. The direction of this stratum is N5°~20°W and its intersection angle with the flow direction is 70°. The rock stratum tilts to the NE (it inclines to the left bank downstream) where the inclination angle is 55°~63°. The dip angle of the rock stratum is 40°. There are faults in four regions in the dam site rock stratum:

- At N5°~20°W, NE∠60° where the region has more than 200 interlayer displacement interfaces. The width of the fracture zone is mainly 10 meters in this region.
- At N30°~60°E, NW∠60° where the average range is 30-50 meters per band.
- At N70°~90°W, NE∠70~85°
- At N65°~80°W, NE∠80° where the fracture zone is relatively wide

2.2.3. Climate

The climate at the location is mild, rainy and sub-tropical. The annual average temperature at the dam site is 20,1°C, the monthly average minimum (January) temperature is 11,0°C and the monthly average maximum temperature (July) is 27,1°C. The rain season stretches between April and October, and it accounts for 89,5% of the annual precipitation and 71,2% of the rain days of the whole year. The average annual precipitation is between 760 ~ 1 860 mm around the basin.

The fetch in the reservoir is 2 km. The annual average wind speed is 0,7 m/s and the maximum annual average wind speed is 13,7 m/s.

2.2.4. Runoff, flood and sediment

The runoff is mainly formed by precipitation. The average annual runoff flow is 1 610 m^3/s and the average total annual runoff is 50,8 billion m^3. The maximum and the minimum average annual runoff flows are 1,42 respectively 0,54 times the average annual runoff flow.

Floods in the basin of the Hongshui River are formed by rainstorms. The magnitude of the rainstorm precipitation during the flood season is not large, but the rainstorms have a high occurrence and therefore often cause flooding.

The sediment in the Hongshui River consists mainly of suspended load, and the suspended sediment is fine. The average annual sediment transport rate at the dam site is 1 660 kg/s with an annual average sediment concentration of 1,05 kg/m^3, which equals to an annual average sediment transport of 52,4 million tons. The height of the sediment accumulating in front of the dam is 92 meters. The unit weight of the sediment is $\gamma_s = 12$ kN/m^3 and the internal friction angle of the sediment is $\phi_s = 24°$.

2.2.5. Design water levels

The normal water level (NWL) (which is established based on the flow requirements downstream for diverse economical purposes, mainly irrigation) in the reservoir is 181,6 meters and the check water level (CWL) is 186,7 meters. The tail water level (TWL) is 30,5 meters and the check tail water level (CTWL) is 65,2 meters.

The elevation of the dam site is +195 m as mentioned before. The elevation of the design water levels can be seen in table 2.

Table 2. Elevations of the design water levels

Water levels	Elevation (m)
NWL	376,6
CWL	381,7
TWL	225,5
CTWL	260,2

2.3. Methodology

The project is divided into three main parts. A first theoretical part that sets the reader in the present situation of hydropower in China, as well as a brief introduction to the theory behind dam structures. The second and third parts handle the calculations and the actual design of the dam.

The second part presents an initial design process behind key aspects of the structure to ensure that the preliminary dimensions of the structure fall within the safety region. Firstly, a flood routing is performed according to the flood control requirements, to obtain the design flow and preliminary dimensions of the dam: height, gate size and spillway length. The preliminary design of the standard overflow and non-overflow sections is then later used for the analytical calculations. These calculations are performed to analyse the dam-foundation interface of the largest non-overflow section of the dam, studying the stability and stress capacity of the structure.

The third and final part presents a more detailed analysis of a FE-model of the dam by using the commercial software suite GeoStudio. This numerical analysis includes a more detailed study of the seepage through the foundation, as well as a more detailed stress analysis of the whole non-overflow section. These results are later compared with the analytical calculations. Finally, conclusions and a summary of the results is presented.

3. Theoretical background

Brief theoretical background of gravity dams, dam safety, spillways and outlets. Also gives an overview of the flood routing calculations, analytical calculations and FEM modelling.

3.1. Different types of dams

Dams can be categorized as gravity, buttress and arch dams. These can also be classified after their construction material, as described in the paragraphs below. Several dam types can be present in one single structure. For example, in long dams, the spillway can be built with concrete while the rest is constructed as an embankment (Linsley et al., 1992).

3.1.1. Embankment dams

Embankment dams are wide dams that are constructed with earth or rocks. They can be constructed very cost-effective with earth moving machines if the natural construction materials can be excavated nearby (Hamill, 2011).

Furthermore, embankment dams can be applied in many different environments. They can be constructed on various types of soils and they do not require a sound rock foundation like other types of dams. But, too soft or weak foundations have a limited capacity to withstand high hydraulic gradients safely. Embankment dams can be built in both wide valleys and relatively steep gorges. If they are designed properly, they can cope with displacements and settlements quite adequately without risk for failure.

However, embankment dams are sensitive to overtopping and internal erosion (Novak et al., 2007). Both of these aspects could lead to a failure if not considered in the design. It is therefore common to construct the spillway separately from the embankment dam. The dams are kept water-tight with an impermeable membrane on the upstream face or an impermeable core.

Embankment dams make up around 83% of the world's large dams (Hamill, 2011).

3.1.2. Concrete dams

Dams that are constructed with concrete are called concrete dams. However, some older dams that are built with masonry can also be included in this category (Novak et al., 2007). Gravity, buttress and arch dams are most commonly made in concrete (Linsley et al., 1992). Concrete dams require sound and stable rock foundations as opposed to embankment dams. They also require more excavation work in order to reach solid rock foundations. However, concrete dams are not sensitive to overtopping and they can incorporate an overflow spillway in the dam structure (Novak et al., 2007).

Gravity Dams

Gravity dams use their self-weight to resist the horizontal hydrostatic pressure from the reservoir that tries to overturn the dam. They can be made of concrete, masonry or rock or earth embankments. Concrete gravity dams make up around 11% of the world's dams.

Concrete gravity dams are usually around 50-150 meters high. When they are over 20 meters high they require a sound rock foundation to deal with the compressive stresses created by the weight of the dam
(Hamill, 2011). They are preferably constructed in wide valleys where the bedrock is located no deeper than five meters underneath the ground surface, but they can also be used in narrow valleys (Novak et al., 2007).

Concrete gravity dams are conventionally constructed by a block-building technique where the concrete is poured in blocks (Linsley et al., 1992). Huge amounts of concrete are used to construct gravity dams which makes them expensive. Another problem with concrete is the shrinkage cracks that can form due to the thermal effects during curing (Hamill, 2011).

Buttress dams

There are different types of buttress dams. One of them is the flat slab type, where either a vertical or angled upstream face slab is supported with downstream buttresses. An angled upstream face slab can give increased stability (Hamill, 2011). Another type is the multiple arch type that consists of a series of arches that allow wider spacing of the buttresses (Linsley et al., 1992). The multiple arch type is used when a valley is too wide for a single arch dam (Hamill, 2011).

Buttress dams usually only use 33-50% of the concrete required for a gravity dam of a similar height. But this doesn't always mean that buttress dams are cheaper than gravity dams because they require more reinforcing steel and formwork (Linsley et al., 1992). Moreover, buttress dams require stronger foundations than gravity dams because of higher contact stresses (Novak et al., 2007).

Arch dams

Arch dams transmit most of the water load to the abutments with arch action, but some of the load is also retained by cantilever action. Arch dams are structurally more efficient than gravity and buttress dams (Novak et al., 2007). They use around 20% of the concrete required for gravity dams and are almost always constructed with reinforced concrete.

Arch dams are only suitable in narrow and steep valleys or gorges. They have high structural requirements on the abutments because of a failure of them can be devastating (Hamill, 2011). The rock foundation needs to be of high strength and uniform quality, especially in the abutments where the loads are higher. Only limited deformation is allowed in the foundation and abutments (Novak et al., 2007). Furthermore, the abutments need to be excavated at the right angles to the thrust to prevent sliding (Linsley et al., 1992).

The crest length of an arch dam is commonly limited to around 10 times of its height. The typical height for a large arch dam is 70-250 meters (Hamill, 2011). Double curvature (cupola) dams are curved in both the vertical and horizontal section. They are regarded as the most complex of the different concrete dam structures (Novak et al., 2007).

Relatively few arch dams have failed in comparison to other dam types (Linsley et al., 1992).

3.1.3. Roller-compacted concrete gravity dams

Roller-compacted concrete (RCC) is mixed with a low cement content, fly ash and fine and coarse gravel which creates a dry and no-slump type of concrete (Linsley et al., 1992). The name of the concrete comes from the construction method that is used when the RCC is placed (Portland Cement Association, n.d.). The RCC is compacted with rollers after it has been spread out in layers that are usually 23 to 45 centimetres thick (Linsley et al., 1992).

RCC is a cheap material that offers sufficient structural performance (Novak et al., 2007). But, the biggest advantage with RCC dams is the relatively short construction time. For example, it only took around 26 months to place the RCC when the Shapai dam in China was constructed. The Shapai dam can be seen in figure 7. The Shapai dam is a 132 meters high and 250 meters long double curvature arch dam. Another interesting fact is that the faster the construction process the better the quality of the RCC (International Water Power & Dam Construction, 2014).

Figure 7. The Shapai dam during construction (Malcolm Dunstand and Associates, n.db)

The construction process of conventional gravity dams must be divided into sequences because of the limitation caused by the thermal effects that occur during the curing of concrete (Novak et al., 2007). However, RCC develops less heat during the curing process due to the smaller amount of cement and

because of the fly ash in the mixture. The effect of this is less cracks and shrinkage during curing (Linsley et al., 1992). Moreover, this enables a continuous construction process when building RCC dams (Novak et al., 2007).

Roller-compacted concrete dams can be up to 60% cheaper to construct than conventional concrete gravity dams due to the lower content of cement used in the concrete and an effective use of machinery (Hamill, 2011). However, one flaw with RCC is that it has a higher permeability than conventional concrete. It is therefore important to include a barrier or wall of conventional concrete on the upstream face of RCC dams, because otherwise the seepage can affect the quality of the structure negatively (Novak et al., 2007).

The first RCC dam that was constructed is the Willow Creek dam in Oregon, USA that was finished in 1982 (Linsley et al., 1992). The Willow Creek dam can be seen in figure 8.

Figure 8. The Willow Creek dam (U.S. Army Corps of Engineers, 2009)

3.2. Spillways and outlets

The purpose of a spillway is to safely discharge floods from the upstream side to the downstream of the dam without causing damage (Hamill, 2011). The spillway can be equipped with crest gates to control the water level in the reservoir and the outflow from the dam, but there are also uncontrolled spillways (Linsley et al., 1992). The spillway design is of high importance since around 30% of all dam failures are caused by deficient spillways and operational problems.

There are several types of spillways: overflow, chute, side-overflow, shaft and syphon. The selection of the spillway design depends on the dam type and size, the terrain at the dam location and the requirements on the dam's operation. Only the overflow spillway will be treated in this report since it is commonly used in concrete dams (Hamill, 2011).

3.2.1. Overflow spillways

An overflow spillway is the section of a dam that allows water to flow over the dam crest. Like already mentioned earlier, overflow spillways are mostly used in concrete dams. But they can also be utilized in embankment dams, if special considerations to prevent the risk of erosion and dam failure are made in the design (Hamill, 2011).

An overflow spillway is ideally designed so that the water can flow smoothly over the crest with minimum turbulence (Linsley et al., 1992). The spillway profile should preferably follow the underside of the aerated nappe, because cavitation might occur if the overflowing water loses contact with the spillway surface (Hamill, 2011). The cavitation and vibration that is caused by a water flow that bounces on and off the overflow spillway can cause severe damage to the dam (Linsley et al., 1992).

3.2.2. Energy dissipation arrangements

Water that passes over the dam crest has a high potential energy that is transformed into kinetic energy as the water flows down the spillway. This energy can be very high and cause erosion and damage if it is not dissipated (Punmia and Pande, 1992). For example, the energy that is dissipated at the Tarbela dam spillways in Pakistan can reach up to 40 000 MW (Novak et al., 2007).

There are mainly two types of methods to dissipate energy from a spillway discharge. One way is to reduce the energy through a hydraulic jump, the other way to dissipate energy is by aeration of a jet and the impact of water on the river bed (Garg, 2006). The energy dissipation can also be divided into five different types that can be combined:

- Dissipation at the spillway surface
- Dissipation in a free-falling jet
- Dissipation at impact to the downstream water
- Dissipation in the stilling basin
- Dissipation at the outflow to the river

Energy dissipation at the spillway surface can be achieved using a rougher spillway surface or by placing baffles at the spillway surface. But there is a risk that comes with these installations, because if they are not aerated cavitation might occur. Stepped spillways can also be used to dissipate energy at the spillway surface, but they are only effective during certain flow conditions (Novak et al., 2007).

In ski-jump spillways the energy is dissipated through a free-falling jet that is aerated and diffused, and during the collision with the river downstream (Garg, 2006). Flip-bucket spillways, which is a variant of the ski-jump spillway, work according to the same principle. The energy is mainly reduced during the collision between the jet and the downstream water, and when air bubbles from the jet and those created during the impact are compressed.

The free-falling jets usually land into plunge pools that are excavated during the construction of the dam or created by only the scour from the impacting jets. To avoid problems with erosion near the dam, the spillway must be designed so that the point of impact occurs as far as possible from the bucket. The free-falling jets can also plunge into a stilling basin.

Stilling basins are the most widely used energy dissipation arrangement. There are different kinds of stilling basins, but the most common one is the hydraulic jump type. The hydraulic jump is the simplest and often the best way to transform super-critical flow into sub-critical flow (that is suitable for the downstream riverbed) in a stilling basin (Novak et al., 2007). However, different designs for the energy dissipator should be considered depending on

the relation between the post-jump depth (y_2) and the tailwater level (TWL) for different discharges (Garg, 2006). Another important aspect to take into consideration is that the turbulent flow that occurs during a hydraulic jump can create large differences in pressure which can lead to cavitation in the basin (Novak et al., 2007).

If the pre-jump depth and the post-jump depth is equal for all discharges the hydraulic jump will always happen at the end of the toe of the spillway. For these circumstances a basin with a concrete horizontal apron is advised to provide protection where the jump takes place.

When the TWL is greater than the post-jump depth for all discharges, the hydraulic jump at the toe is reduced by the higher tail water and the energy dissipation is not very efficient. To deal with this problem a sloping apron above the river bed can be used which will allow for a proper jump to happen at a point on the apron where y_2 is equal to the TWL. Another solution is a roller bucket arrangement, where the energy is dissipated by internal turbulence that will occur in two rollers.

For the case when the post-jump depth is always greater than the TWD a sloping apron below the riverbed can be used to obtain the hydraulic jump, because at some point on the apron y_2 will be equal to the TWL. Another option is to construct a so-called subsidiary dam downstream of the main dam. The idea is to raise the TWL downstream of the main dam so that a hydraulic jump can occur at the toe of the main dam. It is also useful to use to use a ski-jump or a flip-bucket arrangement when the TWL is low.

If the relation between the post-jump depth and the TWL varies with the discharge, a sloping apron that is going both above and below the riverbed can be used. By this, there are proper conditions for a hydraulic jump to form both when the TWL is greater than the post-jump depth and vice versa. It is also necessary to construct a horizontal apron and an end sill for this type of configuration (Garg, 2006).

All the energy in the discharge is not reduced in the stilling basin and a consequence of this is that there is always some erosion downstream of the dam. It is practically very difficult and very costly to dissipate all the energy.

The main task of the stilling basin is to keep the dam safe by controlling and decreasing, but not to completely reducing, the scour (Novak et al., 2007).

3.2.3. Bottom flow energy dissipation

When the spillway outlet is located below the tailwater, the energy in the discharge can be reduced by using blocks and sills or guidewalls before the entry to the basin and just downstream of the outlet or in the basin itself. Another method is to lower the soffit of the outlet as the outlet gets gradually wider. The advantage with the second method is that no cavitation or abrasion occurs.

It is important to design the widening of the outlet in a satisfactory manner so that the flow is distributed sufficiently even and so that the distribution of flow continues at the same rate in the stilling basin.

There are also so called ‘’sudden expansion energy dissipators’’ which work by the principle that the energy level in the discharge is reduced when the flow enters larger spaces (Novak et al., 2007).

3.2.4. Outlet works

Outlet works are openings in the dam that are used to get water from the reservoir for various reasons. Most of the reservoir water is underneath the dam crest level and outlet works makes it possible to use the water whenever necessary (Linsley et al., 1992). Outlets are also used to flush away sediment from the reservoir (Novak et al., 2007).

3.2.5. Gates

Gates can be classified after their position in the dam, their function, mode of operation, pressure transmission, types of motion and the type of mechanism. However, the key parameter behind the structural design of a gate is the way that the gate is supposed to transfer the pressure from the water load. There are three main methods to distribute the pressure (Novak et al., 2007):

- Plain vertical lift gates and stop-logs, radial gates and roller gates distribute the stress to the piers and abutments
- Drum gates, bear-trap gates, flap gates, roll-out gates and inflatable gates are transferring the pressure to the sill
- Some types of flap-gates and pontoon gates are transmitting the pressure to both piers and the sill

3.3. Design principles

The numerical analysis is conducted with a commercial software suite that is called GeoStudio. GeoStudio is developed by GEOSLOPE International Limited which is a company that was founded in 1977 and is based in Calgary, Canada (GEOSLOPE, n.da). The programs in GeoStudio can be used for finite element analysis of seepage, stress and deformation, earthquake and dynamic loading, heat and mass transfer as well as slope stability analysis (GEOSLOPE, n.db). This can be utilized in the design and analysis of projects like dams, embankments, walls, slopes, excavations, open pit mines, roads, bridges and more (GEOSLOPE, n.db).

In this project the SEEP/W and the SIGMA/W softwares in GeoStudio have been used to conduct a seepage analysis and stress analysis respectively. SEEP/W is a finite element software that is used for groundwater flow analysis and pore-water pressure analysis. SIGMA/W is a finite element software that is used for stress and deformation analysis of soils and structural materials (Otte, 2018).

3.4. Design flow – flood routing

The design flood of the project is routed through the reservoir to obtain the maximum discharge over the spillways during the event. In turn, this maximum discharge determines the design flow for the project.

Flood routing is used to calculate the maximum height the water reaches in the reservoir during the design flood. This is done taking into consideration the maximum discharge over the spillways and the storage capacity of the reservoir, in order to obtain the complete outflow hydrograph during a flood event. One method that can be used to perform flood routing is the storage indication method. This method applies the continuity equation, equation 1, to establish a relationship between the inflow, the storage of the reservoir and the outflow capacity of the spillway (NRCS, 2004).

$$Q_{in} - Q_{out} = \frac{dV}{dt} \tag{1}$$

where Q_{in} and Q_{out} are respectively the water flowing in and out of the reservoir, both in cubic meters per second, and V is the reservoir storage

volume in cubic meters. Equation 1 can be rewritten to a finite differential form as:

$$\frac{V_2 - V_1}{\Delta t} = \frac{Q_{in,1} - Q_{in,2}}{2} - \frac{Q_{out,1} - Q_{out,2}}{2} \quad (2a)$$

or as:

$$\frac{2V_2}{\Delta t} + Q_{out,2} = Q_{in,1} + Q_{in,2} + \frac{2V_1}{\Delta t} - Q_{out,1} \quad (2b)$$

All the variables on the right-hand side of equation 2b are known, while the time increment (Δt) is set and the remaining variables on the left-hand side are unknown. The unknowns can be easily determined based on the assumption that the storage volume and the outflow depend only on to the water level (it is assumed that the water surface is always level in the reservoir). The outflow differs depending on the reservoir area and the spillway type and size, making flood routing an iterative process, since the spillway in turn, is designed after the outflow (Novak et al., 2007).

3.5. FE-modelling in GeoStudio

Many of the physical phenomena found when working with engineering problems can be described with differential equations. In many cases, these problems are too difficult to solve by using analytical methods. The finite element method is a method where differential equations are solved numerically to approximate the physical behaviour of different bodies or regions.

The method is based on that the body or region of interest is divided into smaller pieces (finite elements) which creates a discrete system with a finite number of unknowns as opposed to a continuous system with an infinite number of unknowns. The differential equations are then solved numerically for each element independently and the solutions are then combined to make an approximation of the physical behaviour of the entire body (Ottosen and Petersson, 1992).

4. Feasibility study

Summary of the feasibility studies required prior a dam project.

4.1. Purpose of dam construction

Several reasons can foment the construction of a dam. However, when studying the possibility of constructing a dam, specific engineering-economic considerations must be met to ensure its real necessity. The project shall always respond to an urgent existing or foreseen social or economic need.

The projected structure shall serve its intended purpose adequately. The services performed and the benefits obtained by the existence of the dam, shall justify its construction cost and the impact on the surrounding environment (USBR, 1987).

In this project, the purposes that drive the construction of the dam are: navigation, flood control downstream, water supply, energy generation and fishery industry enhancement.

4.2. Selection of dam type

The selection of the dam type is governed by two main aspects. These are, the geology of the area where the dam is to be constructed and the economic resources available for the project. Novak et al. (2007), states the following considerations as the four primal ones to think of when selecting the type of dam: the nominal value of the hydraulic gradient, the nominal stresses transmitted to the foundation, the foundation deformability and the required foundation excavation.

The first two aspects, the hydraulic gradient and the nominal stresses, can vary by one order of magnitude depending on the type of dam. Although embankment dams have less requirements regarding foundation quality compared to concrete dams, the softer and more erodible foundations present limited ability to safely resist high hydraulic gradients.

Regarding the third aspect, certain types of dams cope better with cracking and stress redistribution as a result of non-uniform foundation deformation and/or settlement. An embankment dam provides higher structural flexibility, opposed to concrete dams. Among the different concrete dam types, gravity dams are more adaptable to any type of foundation. Arch dams are not appropriate for faulty geology since they are sensitive to differential settlements that can cause cracks carrying to the collapse of the structure. This is due to the way the arch dam transmits the loads. In arch dams, the pressure from the water body is transmitted to the bedrock mainly horizontally through the abutments; while in gravity dams, they are transmitted vertically downwards through the foundation. The fourth aspect shows a preference for embankment dams over concrete dams, because of the excessive excavation volumes required to reach deep rock-solid foundations needed for the latter type. However, as stated previously, the selected type of dam must be concrete, due to the hydropower requirement, making this last aspect less relevant. Even though excavations will be required, the selection of the site for the location of the dam, shall be such that minimises the volume of excavation needed.

Depending on the geological conditions different types of dams are suitable. Earthfill dams can be used in wide valleys and they are appropriate for both rock and soil foundations. Furthermore, they can cope with small settlements if designed and constructed properly. Earthfill dams are, however, sensitive to soils with high permeability and special considerations against seepage must be taken. Gravity dams are suitable for wide valleys as well, under the condition that there is bedrock located no deeper than five meters beneath the ground surface (Novak et al., 2007). Another important aspect when designing gravity dams is the state of the rock foundation, it must be ensured that no sliding occurs.

When designing buttress dams the same aspects are of importance as for gravity dams. However, since there will be higher contact stresses in buttress dams there are higher requirements on the structural capacity of the bedrock for these types of dams.

Rockfill dams are also favourably constructed on rock foundations but the rock can be of varying quality. On the other hand, special measures against seepage must be taken when designing rockfill dams.

Arch dams are suitable in narrow gorges. It is important that the rock foundation is of high strength and of uniform quality because arch dams' sensitivity to settlements, especially in the abutments where the loads are higher.

The selected structure type for the present project is a hydropower roller-compacted concrete gravity dam. It can be concluded that this type of dam presents several advantages over the other concrete dam alternatives. Gravity dams do not have a strict requirement on the quality of the rock foundation, being more flexible to settlements and deformations. They can adequately cope with high hydraulic gradients. What is more, the construction process is more straightforward and less complex than the other alternatives.

4.3. Site selection

When determining the location of the dam many factors should be taken into account. Narrow valleys are ideal locations to reduce the length of the structure and thus the construction cost. It is preferable to choose a site where the bedrock is nearest to the surface, to reduce economical expenses of deep foundation and excavation of the superficial terrain. Also, to avoid large excavations costs, natural reservoir formations are favoured. In general, jointed faulted rock is to be avoided.

Some local factors involving the general feasibility of the construction of the project must be added to the evaluation of the selection of the site. Some of these factors are: availability of nearby construction material, access to the remote location, enough space for adjacent facilities such as concrete plant, safe means of river diversion during construction to ensure a low risk working environment.

5. Flood routing

Application of the storage indication method to route the 500- and 10.000-year floods through the reservoir. Definition of the preliminary dimensions of the structure.

5.1. Inputs to the storage indication method

The first step to design a dam is to set the design flow (reservoir inflow) hydrograph used for the calculations. In the present report, the probable maximum flood (PMF) is given and it is obtained as a multiple of the floods associated to certain return periods. Given the dam category is A, meaning that dam failure would endanger lives in a community (Novak et al., 2007), the return period shall be 10 000 years.

The inflow hydrographs for the 500-year and 10 000-year return period floods are given and can be seen in figure 9 and figure 10 respectively.

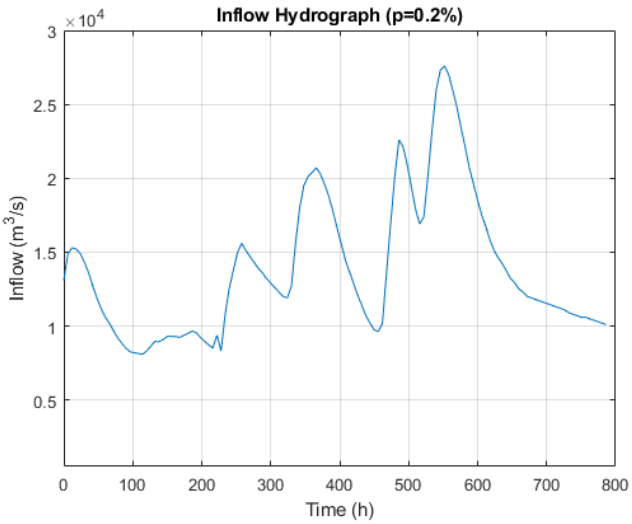

Figure 9. Hydrograph for 500-year flood (p=0,2%).

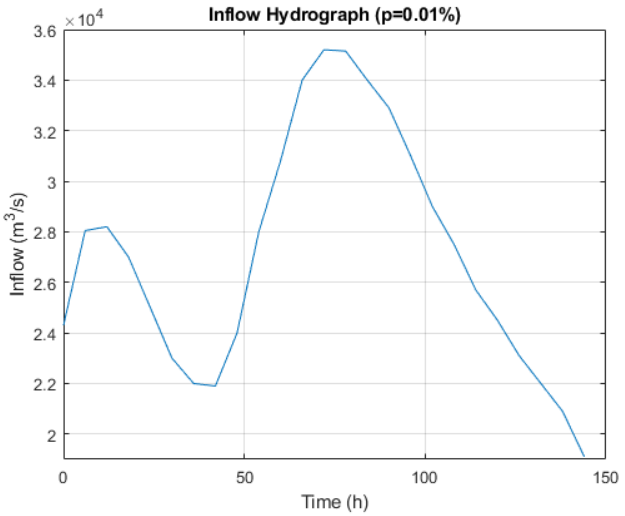

Figure 10. Hydrograph for the 10 000-year flood (p=0,01%).

Figure 11 includes the plot of the relation between the water elevation or stage against the storage volume in the reservoir.

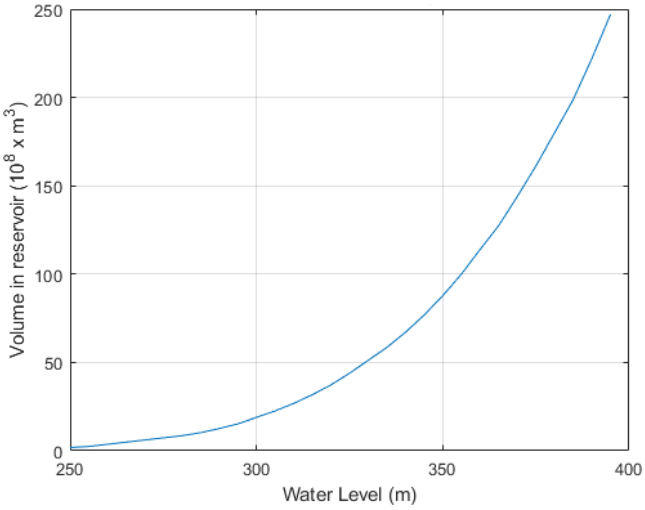

Figure 11. The volume in the reservoir plotted against the water level.

5.2. Flood routing calculation

The flood routing calculations are performed using the excel sheet in table 4. The inputs needed to execute a flood routing are: the flood hydrographs (figure 9 and 10), the stage-storage curve of the reservoir (figure 11), the stage-discharge relationship (equation 3) and the starting elevation.
The discharge through the gate is defined by equation 3:

$$Q_{out} = KBH^{\frac{1}{2}} \tag{3}$$

where Q_{out} is the outflow through an orifice or gate in cubic meters per second, B is the orifice or gate width in meters, H is the water head from the centreline of the orifice or gate to the free water surface upstream measured in meters, and K is a constant that includes the discharge, submerge and shrinkage coefficients. Values for the outflow coefficient K are obtained from *Hydraulic structures* by Sheng-Hong Chen (2015) and are included in table 3:

Table 3. Values for outflow coefficient K

Design condition	K=$\sigma\varepsilon$m
NWL	2,01
CWL	2,04

The starting elevation is the top of the joint use capacity for flood control and normal service conditions. The flood capacity level (FCL) and the normal water level (NWL) are equal to 376,6 m. The NWL is established based on the flow requirements downstream for diverse economical purposes, mainly irrigation. The time-step is set to 6 hours, which is also the time step used in the hydrographs. The flood routing starts when the inflow surpasses the discharge capacity of the spillway (with the gates fully opened) and water starts accumulating in the reservoir, rising the water surface elevation.

Columns 2 and 3 indicate the water coming into the reservoir that is obtained from the hydrograph for the 500-year flood (figure 9). Column 5 is the water going out of the reservoir through the gated spillway, computed with equation 3 and an estimated water head in column 11. The average inflow and average outflow are calculated in columns 4 and 6 respectively. These values are used

to calculate the water storage increment in column 7, by applying the continuity equation (equation 2a). The final water storage volume is obtained by adding the water storage increment to the existing volume of water in the reservoir in column 8. The water elevation in the reservoir in column 9 is obtained by linear interpolation of the value in column 8 with the stage-storage curve of the reservoir (figure 11), included in columns 13 and 14. This last value is compared to the previously estimated water head in column 11, both values should not differ in more than 10 cm. Column 12 is the distance between the water surface at a certain time step and the NWL.

Table 4. Excel sheet used for the flood routing calculations

1	2	3	4	5	6	7	8	9	10	11	12	13	14
i	Time t(h)	Inflow Q_{in} (m^3/s)	Average Inflow ΔQ_{in} (m^3/s)	Outflow Q_{out} (m^3/s)	Average outflow ΔQ_{out} (m^3/s)	Reservoir water storage increment ΔV (10^8 m^3)	Water storage V (10^8 m^3)	Reservoir level z(m)		Estimated water level at the end of the period z(m)	Head of the overflow H_1 (m)	Water level (Elevation on stage) z(m)	Reservoir volume (Storage) V (10^8 m^3)
0	0	0		0			167,25	181,60		181,60	0,0	**180**	**161,250**
0	0	0	0	0	0	0,00	167,25	181,60		181,60	0,0	**185**	**180,000**
0	0	20 200	0	17 673	0	0,00	167,15	181,60		181,60	0,0	**190**	**198,750**
1	6	23 300	21 750	17 993	17 833	0,85	168,10	181,83		181,80	0,2	**195**	**221,951**
2	12	26 000	24 650	18 639	18 316	1,37	169,46	182,19		182,20	0,6	**200**	**246,951**
3	18	27 300	26 650	19 293	18 966	1,66	171,12	182,63		182,60	1,0		
4	24	27 600	27 450	20 121	19 707	1,67	172,80	183,08		183,10	1,5		
5	30	27 000	27 300	20 792	20 457	1,48	174,27	183,47		183,50	1,9		
6	36	25 900	26 450	21 300	21 046	1,17	175,44	183,78		183,80	2,2		
7	42	24 800	25 350	21 641	21 470	0,84	176,28	184,01		184,00	2,4		
8	48	23 400	24 100	21 812	21 726	0,51	176,79	184,14		184,10	2,5		
9	54	22 100	22 750	21 983	21 897	0,18	176,98	184,19	peak	184,20	2,6		
10	60	20 700	21 400	21 983	21 983	-0,13	176,85	184,16		184,20	2,6		
11	66	19 600	20 150	21 641	21 812	-0,36	176,49	184,06		184,00	2,4		
12	72	18 500	19 050	21 470	21 555	-0,54	175,95	183,92		183,90	2,3		
13	78	17 500	18 000	21 130	21 300	-0,71	175,24	183,73		183,70	2,1		
14	84	16 700	17 100	20 792	20 961	-0,83	174,40	183,51		183,50	1,9		
15	90	15 800	16 250	20 456	20 624	-0,94	173,46	183,26		183,30	1,7		
16	96	15 100	15 450	19 955	20 205	-1,03	172,43	182,98		183,00	1,4		
17	102	14 600	14 850	19 458	19 706	-1,05	171,38	182,70		182,70	1,1		
18	108	14 200	14 400	18 965	19 212	-1,04	170,34	182,42		182,40	0,8		
19	114	13 700	13 950	18 477	18 721	-1,03	169,31	182,15		182,10	0,5		
20	120	13 200	13 450	18 154	18 315	-1,05	168,26	181,87		181,90	0,3		
21	126	12 900	13 050	17 673	17 913	-1,05	167,21	181,59		181,60	0,0		

As shown in figure 12, the capacity of the reservoir temporarily increases during the flood event, since the opening of the gates allows a higher water level. This volume cannot be retained in the reservoir and will flow out until the flood control level is reached again.

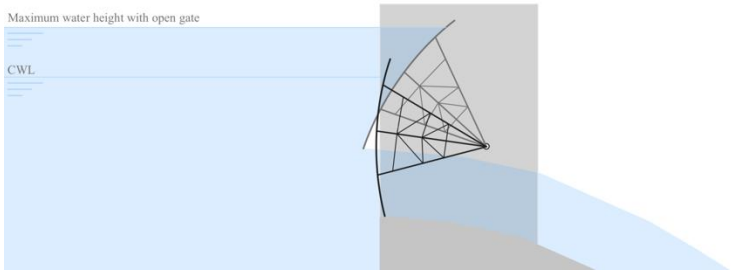

Figure 12. Schematic drawing showing the concept of surcharge

Several spillway lengths and weir crest elevations are modelled to finally obtain the optimum spillway length of 130,0 m and the weir crest elevation of 360,0 m.

The maximum outflow occurs when the discharge equals the inflow, marked by the intersection point of both curves shown in figure 13 and figure 14 for the 500- and 10 000-year flood respectively. The maximum discharge of 21 983 m^3/s occurs 54 hours after the routing start. The surcharge, maximum water height above the NWL reached during the flood event, is 2,6 m. When routing the 10 000-year flood through the reservoir, the maximum discharge of 26 808 m^3/s occurs 66 hours after the routing starts and the maximum reached height is 5,1 m above CWL.

Following the requirements downstream and the capacity of the river, the maximum allowable discharge is 250 $m^3/s/m$. Thus, for a 130 meter-long opening the maximum discharge is 32 500 m^3/s, which is higher than the peaks during both flood events.

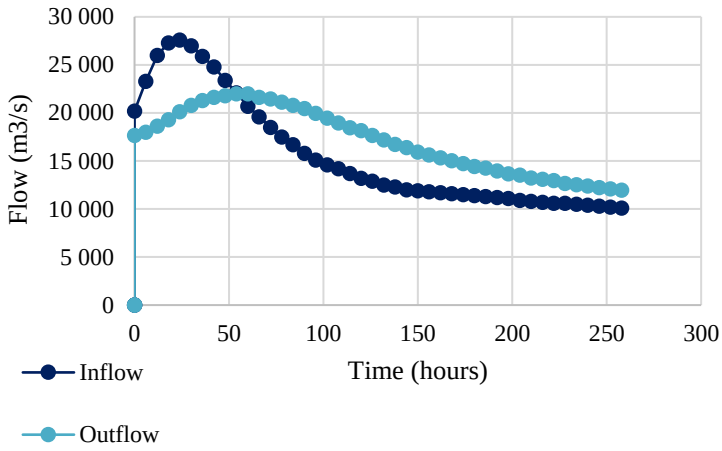

Figure 13. Plot of the 500-year flood hydrograph against the discharge hydrograph during the flood routing

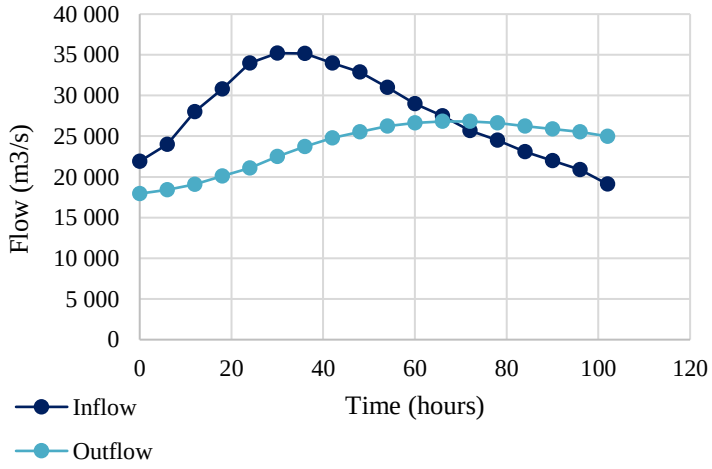

Figure 14. Plot of the 10 000-year flood hydrograph against the discharge hydrograph during the flood routing

6. Design of non-overflow section

Design of the non-overflow section and determination of the freeboard and parapet height. Equations to calculate the freeboard and standard values for NOF profile design are extracted from "Hydraulic Structures" by Sheng Hong Chen (2015) and the Chinese Standard (SL319-2005) "Design Specification for Concrete Gravity Dams".

The design of the non-overflow (NOF) section is mainly the design of the freeboard that is the vertical distance between the highest point of the dam (top of the parapet or wave-wall) and the full supply level in the reservoir (Novak et al., 2007).

According to Sheng Hong Chen the freeboard Δh is calculated as the combined effects of wave action and run-up, wind set-up of the water surface and flood routing. All of these phenomena produce a temporary rise of the reservoir water surface and shall be taken into consideration so that overflow above the dam crest does not occur. Then, the freeboard is computed with equation 4 as:

$$\Delta h = h_{1\%} + h_z + h_c \tag{4}$$

where $h_{1\%}$ is the wave height with 1% cumulative frequency in meters, h_z is the height of wave induced surge in meters and h_c is extra height added as a safety method depending on the dam grade measured in meters. The grade of the designed dam is I, accordingly, the safe extra height h_c is 0,7 m for NWL conditions and 0,5 m for CWL conditions.

The wave height $h_{1\%}$ is computed with table 5 from the wave height associated to a cumulative frequency of 2% which is calculated with equation 5:

$$\frac{g h_{2\%}}{{v_0}^2} = 0{,}00625 {v_0}^{1/6} \left(\frac{gD}{{v_0}^2}\right)^{1/3} \tag{5}$$

where v_0 is the wind speed in meters per second, D is the wind zone length or fetch in kilometres and g is the gravitational acceleration in meters per square

second. The wind speed has different values regarding the design scenario, being equal to the maximum calculated wind speed v_{max} under CWL conditions and 1,5 times this value under NWL conditions. The multi-year average of maximum wind speed v_{max} for the designed structure is 14 m/s^2, so v_0 is 21 m/s^2 for CWL and 14 m/s^2 for NWL. The wind fetch is 2 km. Therefore, $h_{2\%}$ is equal to 0,09 m for CWL and 0,17 m for NWL conditions.

$h_{1\%}$ is determined by the ratio between the wave height for a certain cumulative frequency and the average wave height which is listed in table 5, where h_m is the average wave height and H_m is the average water depth.

Table 5. Ratio between the wave height for different cumulative frequencies and the average wave height. Obtained from Chinese Standard (SL319-2005)

$\frac{h_m}{H_m}$	$p\%$									
	0,1	1	2	3	4	5	10	13	20	50
0	2,97	2,42	2,23	2,11	2,02	1,95	1,71	1,61	1,43	0,94
0,1	2,70	2,26	2,09	2,00	1,92	1,87	1,65	1,56	1,41	0,96
0,2	2,46	2,09	1,96	1,88	1,81	1,76	1,59	1,51	1,37	0,98
0,3	2,23	1,93	1,82	1,76	1,70	1,66	1,52	1,45	1,34	1,00
0,4	2,01	1,78	1,68	1,64	1,60	1,56	1,44	1,39	1,30	1,01
0,5	1,80	1,63	1,56	1,52	1,49	1,46	1,37	1,33	1,25	1,01

Given that h_m is several orders of magnitude smaller than H_m, it can be safely assumed that the ratio between both of them is less than 0,1. Entering table 5 with h_m/H_m=0,1 and p=2%, it is obtained $h_{2\%}/h_m$=2,09. Given the calculated values of $h_{2\%}$, h_m is equal to 0,04 m for CWL and 0,08 m for NWL conditions. Entering table 5 again but with p=1%, it is obtained $h_{1\%}/h_m$=2,26. Thus, $h_{1\%}$ is equal to 0,10 m for CWL and to 0,18 m for NWL conditions.

The height of wave induced surge or the distance between the wave centreline and the NWL or the CWL (depending on the design scenario) is calculated with equation 6:

$$h_z = \frac{\pi {h_{1\%}}^2}{L_m} cth \frac{2\pi H}{L_m} \quad (6)$$

where $h_{1\%}$ is the wave height with 1% cumulative frequency in meters calculated previously, H is either the NWL or the CWL plus their respective flood surcharge in meters and L_m is the wave length in meters calculated with equation 7:

$$\frac{g L_m}{{v_0}^2} = 0{,}0386 \left(\frac{gD}{{v_0}^2}\right)^{1/2} \quad (7)$$

where v_0 is the wind speed, D is the wind zone length or fetch in kilometres and g is the gravitational acceleration in meters per square second. Using the values of D and v_0 previously calculated L_m is equal to 0,24 m for CWL and 0,37 m for NWL conditions. Applying equation 6, h_z is equal to 0,12 m for CWL and equal to 0,27 m for NWL conditions.

Applying equation 4, the freeboard is 0,7 m for CWL conditions and 1,2 m for NWL conditions.

The total height of the dam is the maximum value between the height at NWL, equation 8a, and the height at CWL, equation 8b.

$$H_n = h_n + \Delta h_n \quad (8a)$$

$$H_c = h_c + \Delta h_c \quad (8b)$$

where h_n is the water surface elevation at NWL, h_c is the water surface elevation at CWL and Δh_n and Δh_c are the freeboards for NWL and CWL respectively. So, H_n is 185,4 m and H_c is 187,4 m. The height of the parapet must satisfy the added condition that it must be at least 1,3 meters tall above

CWL. Considering this last condition and knowing that the CWL is 186,7 m, the total height of the dam is 188,0 m.

The possible profiles of the NOF section may be divided into three basic types depending on the shape of the upstream face: vertical, partially inclined (battered), inclined. The second type is the chosen one in this design, due to its increased sliding resistance thanks to the extra weight provided by the water. Following standard values, the upstream wall has a slope of 0,15 and the downstream wall has a slope of 0,75. As previously calculated, the height of the dam is 188,0 meters. It is recommended that the width of the crest falls between 8-10% of the total height of the dam and always thicker than 2 meters. Complying with these requirements, the main dimensions of the NOF section are presented in table 6 and figure 15.

Table 6. Non-overflow section main dimensions

Dimension	Symbol	Value
Dam height	h_{dam}	188,0 m
Bottom thickness	T_{dam}	149,4 m
Crest thickness	t_{crest}	18,8 m
Upstream wall slope	n	0,15
Downstream wall slope	m	0,75

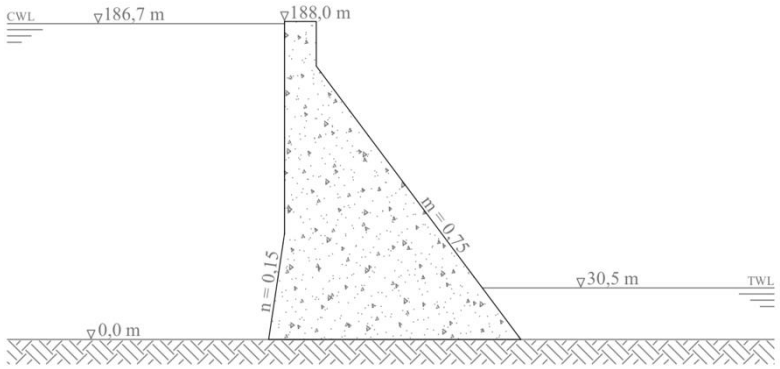

Figure 15. Cross-section of NOF section during CWL condition

7. Design of overflow section

Design of the overflow section following the provisions from the US Army Waterways Experimental Station.

The overflow section requires the capacity to safely discharge floods and to dissipate the large amount of energy from the outflow. Longtan dam uses an overflow spillway with a trajectory bucket as the energy dissipation arrangement, which is why the same configuration has been designed in this report.

The crest profile of the spillway was designed with the provisions from the U.S. Army Waterways Experimental Station according to figure 16 and equation 9:

$$y^{1,85} = 2{,}0 \cdot H_{h,d}^{0,85} z \tag{9}$$

where $H_{h,d}$ is the design head value, which is 75%-95% of the maximum head, $H_{h,max}$ (Novak et al., 2007).

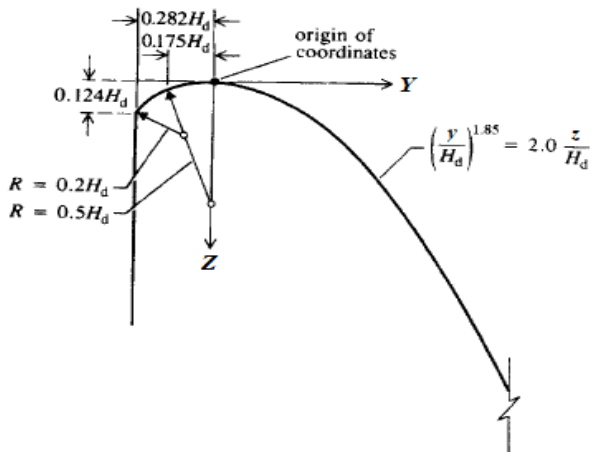

Figure 16. Crest profile of an ogee spillway (U.S. Army Waterways Experimental Station, 1959)

After 27,97 meters in the y-direction and 20,98 meters in the z-direction in reference to figure 16, the spillway takes on the slope of 1:0,75. This was determined with the following operations:

$$y^{1,85} = 2,0 \cdot H_{h,d}^{0,85} z$$

$$\rightarrow z = \frac{y^{1,85}}{2,0 \cdot H_{h,d}^{0,85}}$$

The derivative of z as a function of y:

$$\rightarrow z' = \frac{y^{0,85}}{2,0 \cdot H_{h,d}^{0,85}}$$

The maximum head value was assumed to be the difference between the CWL and the spillway crest level, which gives the following design head value:

$$H_{h,d} = 0,8 \cdot (186,7 - 165) = 17,36\, m$$

To determine when the curve takes on the slope of 1:0,75, the y-value for z'=1:0,75 had to be determined:

$$y = \left(\left(\frac{1}{0,75}\right) \cdot 2 \cdot 17,36^{0,85}\right)^{\frac{1}{0,85}} = 27,97\, m$$

To get the corresponding z-coordinate, the y-value of y=27,97 was inserted into equation 9.

It is recommended that the flip angle of the flip-bucket is between 20° to 40° and that the tailwater elevation should be well below the bucket (Rajan and Shivanshankara Rao, 1980). Furthermore, the minimum bucket radius should be three to five times the approach flow depth in the bucket (Mason, 1993). Since the downstream check water level is 260,2 meters, the elevation of the flip bucket was set to 262,2 meters. The bucket angle was set to 35° and the bucket radius was chosen as $12,4d_0$, where d_0 is the water depth at the lowest

point of the arc when the gates are fully opened during the 500-year flood. d_0 was determined with equation 10:

$$d_0 = \frac{Q_{500}}{B \cdot v} \tag{10}$$

where B is the spillway length and Q_{500} is the discharge during the 500-year flood. The velocity, v, is determined according to equation 11 taken from the Chinese Standard DL5108-1999:

$$v = \varphi \cdot \sqrt{2 \cdot g \cdot H_0} \tag{11}$$

where H_0 is the difference between bucket elevation and the reservoir level. H_0 was assumed to be the difference between the bucket elevation and the peak reservoir level during the 500-year flood, which can be found in the flood routing chapter. φ is a reduction factor that is set to 95% to account for the energy losses on the spillway surface. The following velocity was obtained:

$$v = 0{,}95 \cdot \sqrt{2 \cdot 9{,}81 \cdot (379{,}2 - 262{,}2)} = 45{,}5\ m/s$$

Since the spillway length is 130 meters, the following value for d_0 was determined during the peak discharge during the 500-year flood:

$$d_0 = \frac{21983}{130 \cdot 45{,}5} = 3{,}7\ m$$

Making the arc radius of the flip-bucket 46 meters.
The trajectory of the free-falling jet was determined with equation 12 taken from the USBR Design Standard No. 14:

$$z = y tan\theta_0 - \frac{y^2}{4k_{tr}h_v \cos^2\theta_0} \tag{12}$$

where the trajectory coefficient, k_{tr}, is equal to 1. θ_0 is the angle of the jet discharging from the flip-bucket and h_v is the velocity head at the bucket brink. The reference point for the y- and z-coordinates is the brink of the flip-bucket.

h_v is determined with equation 13:

$$h_v = v_b^2/2g \tag{13}$$

where v_b is the brink velocity that for concrete dams is determined with equation 14:

$$v_b = 0{,}808 \cdot \left(2gH_{h,tot}\right)^{0{,}5} \tag{14}$$

where $H_{h,tot}$ is the total head.

The results below describe the trajectory of the free-falling jet when the total head, $H_{h,tot}$, is set as the spillway crest level. The discharge angle, θ_0, is equal to the bucket angle of 35°.

$$v_b = 0{,}808 \cdot (2 \cdot 9{,}81 \cdot 165)^{0{,}5} = 46\ m/s$$

$$\rightarrow h_v = \frac{46^2}{2 \cdot 9{,}81} = 108\ m$$

With these values, the jet plunges into the downstream when y = 245 meters and z = -36,7 meters under conditions where the tailwater elevation is 225,5 meters (i.e. when the tailwater level is 30,5 meters). The peak of the jet is located at y=101 meters and z=35,4 meters (i.e. the peak of the nappe is elevated 35,4 meters above the brink of the bucket).

The scour depth from the free-falling jet can be estimated with equation 15 taken from the Indian Standard IS 7365:2010:

$$d_s = 1{,}9H_3^{0{,}225}q^{0{,}54} \tag{15}$$

where d_s is the scour depth in meters, H_3 is the difference between the reservoir level and tailwater level in meters and q is the specific discharge in $m^3/s/m$. It was assumed that H_3 is the difference between the spillway crest level and the tailwater level.

The scour depth was computed by using the peak discharge during the 500-year flood and assuming that the tailwater level is 30,5 meters, which gave the following result:

$$d_s = 1{,}9 \cdot (165 - 30{,}5)^{0{,}225} \cdot \left(\frac{21983}{130}\right)^{0{,}54} = 91{,}4\ m$$

The height of the spillway sidewalls was determined with equation 16 taken from Garg (2006):

$$h_{sidewall} = 0{,}61 + 0{,}04v \cdot d_0^{\frac{1}{3}} \tag{16}$$

The velocity and the depth of the water that had been determined previously gave the following result:

$$h_{sidewall} = 0{,}61 + 0{,}04 \cdot 45{,}5 \cdot 3{,}7^{\frac{1}{3}} = 3{,}42\ m$$

The cross-section of the overflow section seen in figure 17 below is a result of the provisions and calculations described in this section.

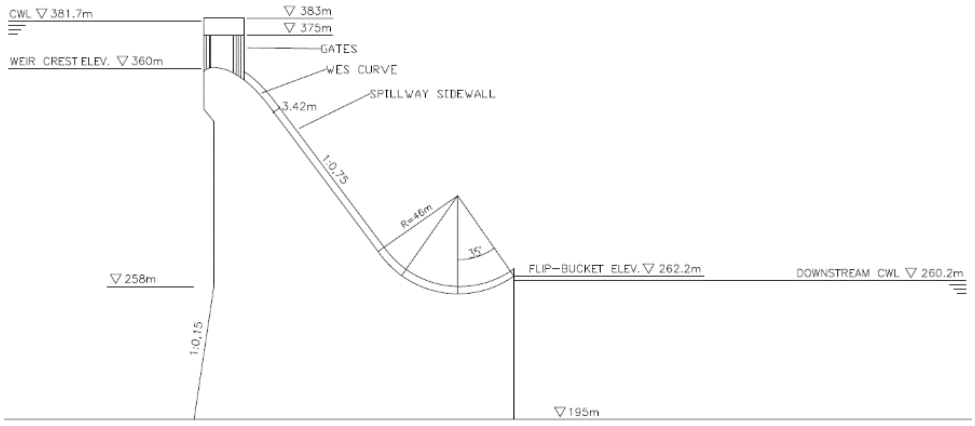

Figure 17. Overflow section

It is important to keep in mind that the cross-section in figure 17 is only an initial design of the overflow section that was obtained with several assumptions and simplifications. The final design of the flip-bucket should be investigated and developed with the help of scale-models. Another important aspect is that the estimated scour is 91,4 meters deep when the tailwater level is only 30,5 meters. Therefore, to protect the riverbed downstream of the dam from uncontrolled scour, either a plunge pool has to be excavated or a stilling basin needs to be constructed where the impact occurs. Furthermore, the point of impact should be studied more extensively as the trajectory of the free-falling jet depends on the total head. It must be ensured that the plunge pool or stilling basin is constructed at the right distance from the dam.

8. Loads acting on the dam

Introduction to the forces present in the analysis of a gravity dam. Description of the magnitude and place of action of each load. Equations for the loads are taken from the text "Hydraulic Structures" by Sheng Hong Chen (2015). The standard values of specific weight of concrete, sediments and water given by the Eurocode are used.

The present report follows the sign convention shown in figure 18.

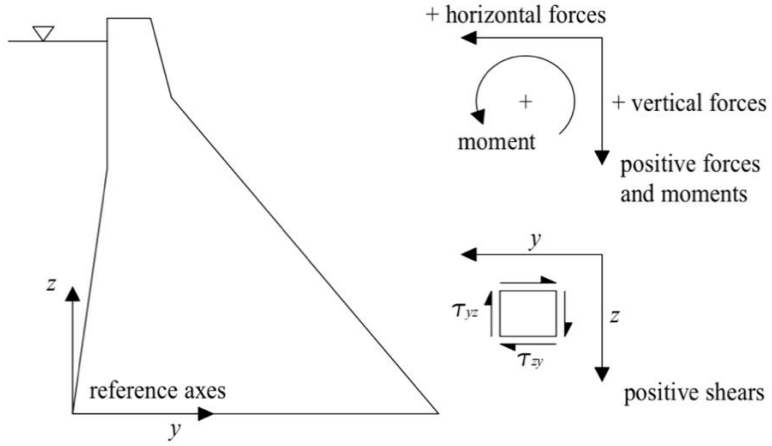

Figure 18. Sign convention

The forces acting on a gravity dam are:

- Dead loads: self-weight of the dam
- Hydrostatic pressure: reservoir and tail water
- Uplift pressures
- Silt pressures
- Dynamic water pressure: wave action
- Earthquake forces
- Seismic dynamic water pressure
- Ice pressure
- Thermal loads

However, given the location of the dam and the nature of calculations being a preliminary design, the ice pressure, the seismic dynamic water pressure and the thermal loads are regarded as negligible. The loads included in the calculations are as follows:

- Self-weight
- Hydrostatic pressure
- Uplift force
- Dynamic water pressure
- Silt pressure
- Earthquake action

The action of these loads is calculated for the non-overflow section (NOF) located in the central area of the dam, where the height is largest. The momentum at M, located in the mid-point of the bottom of the dam, created by each load is calculated as well.

8.1. Self-weight of the dam

The self-weight (figure 19) is determined according to equation 17:

$$G = A \cdot \gamma_c \tag{17}$$

where, A is the area of the NOF cross-section in square meters and the specific weight of concrete is $\gamma_{concrete} = 24{,}0$ kN/m^3.

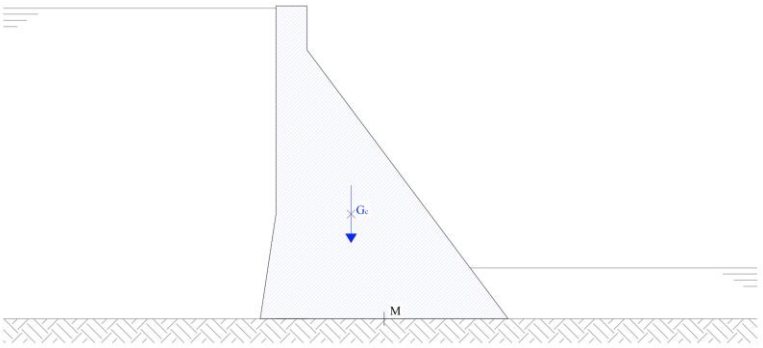

Figure 19. Self-weight

The area is determined by dividing the cross-section into three parts (figure 20): the heel, the mid-section and the toe. The area of each part as well as the total area for the whole cross section can be seen in table 7.

Table 7. Cross-sectional area of NOF section

	Width [m]	Height [m]	Area [m^2]
Heel	9,40	62,67	294,53
Mid-section	18,80	188,00	3 534,40
Toe	121,23	161,63	9 797,00
			Σ=13 626,00

The contribution to the moment in point M by each part is calculated with equation 18:

$$M_i = G_i \cdot x_i \tag{18}$$

where G_i is the dead-load of each part respectively and x_i is the distance between each part's center of gravity and the point M computed in meters. Point M is located at the mid-point of the base of the dam.

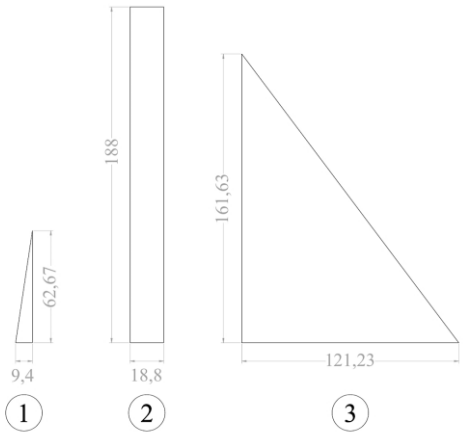

Figure 20. Dam subdivisions used to calculate the self-weight

8.2. Hydrostatic pressure

The horizontal hydrostatic pressure (figure 21) on the dam is determined with equation 19a:

$$P_{horizontal} = \frac{1}{2} \cdot \gamma_w \cdot H^2 \qquad (19a)$$

where the unit weight of water is $\gamma_w = 10$ kN/m^3 and H is the water depth in meters.

The vertical hydrostatic pressure (figure 21) is determined by calculating the area of water, A_w, that is located above the heel and the toe respectively, as shown in equation 19b:

$$P_{vertical} = A_w \cdot \gamma_w \qquad (19b)$$

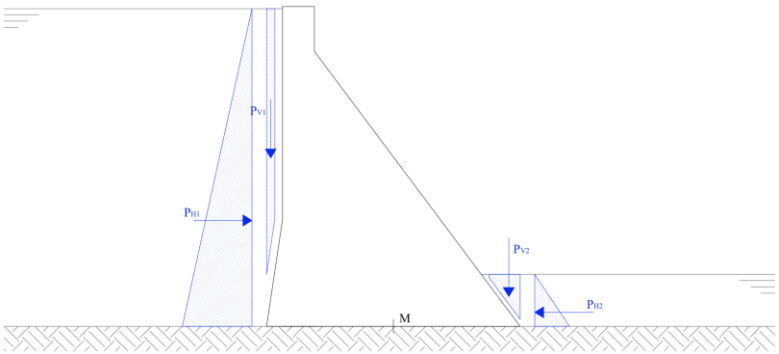

Figure 21. Hydrostatic pressure

8.3. Uplift force

In order to reduce the uplift pressure, two curtains are located seven meters away from the heel and the toe of the dam. The pressure attenuation at those points is described by the coefficient α, chosen according to Chinese Standards (table B.3.1 in *Design Specification for Concrete Gravity Dams* (SL319-2005)), equal to:

$$\alpha_{upstream\ curtain} = 0{,}2$$

$$\alpha_{downstream\ curtain} = 0{,}5$$

The uplift pressure (figure 22) is computed with the following equation 20:

$$p_{uplift} = \alpha \cdot \gamma_w \cdot H \qquad (20)$$

where H is the water level and α is the pressure attenuation coefficient.

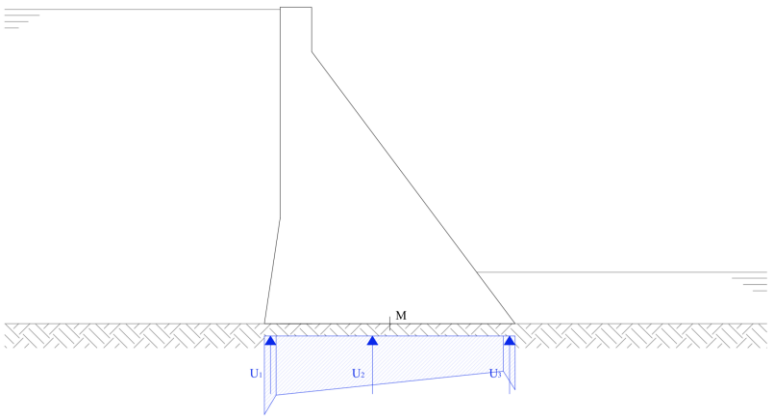

Figure 22. Uplift force

8.4. Silt pressure

The sediments that accumulate in front of the dam will create pressure (figure 23) that can be determined with the following equations 21a and 21b:

$$P_{sk,horizontal} = \frac{1}{2} \cdot \gamma_s \cdot h_s^2 \cdot \tan^2\left(45° - \frac{\phi_s}{2}\right) \quad (21a)$$

$$P_{sk,vertical} = \frac{1}{2} \cdot h_s^2 \cdot n \cdot \gamma_s \quad (21b)$$

where the floating bulk density of the sediment is $\gamma_s = 12$ kN/m^3, the sediment deposition thickness in front of the dam is $h_s = 92$ m, the internal friction angle of the sediment is $\phi_s = 24°$ and the slope of the heel is $n = 0{,}15$.

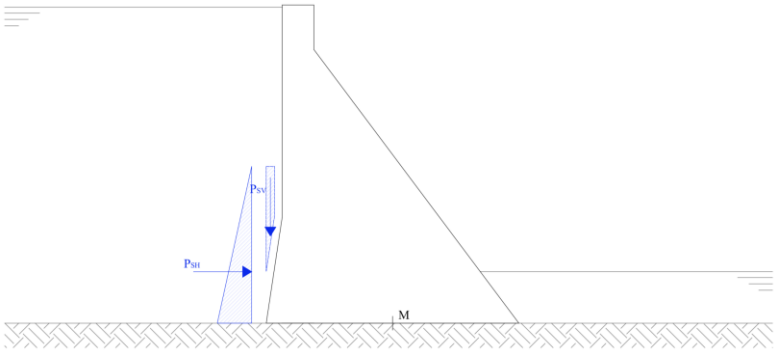

Figure 23. Silt pressure

8.5. Dynamic water pressure

The pressure from waves (figure 24) is calculated according to equation 22:

$$P_{wk} = \frac{1}{4} \cdot \gamma_w \cdot L_m \cdot (h_{1\%} + h_z) \quad (22)$$

where γ_w is the unit weight of water, L_m is the wave length, $h_{1\%}$ is the wave height with a cumulative frequency of 1% and h_z is the height difference between the central line of the wave during NWL and CWL.

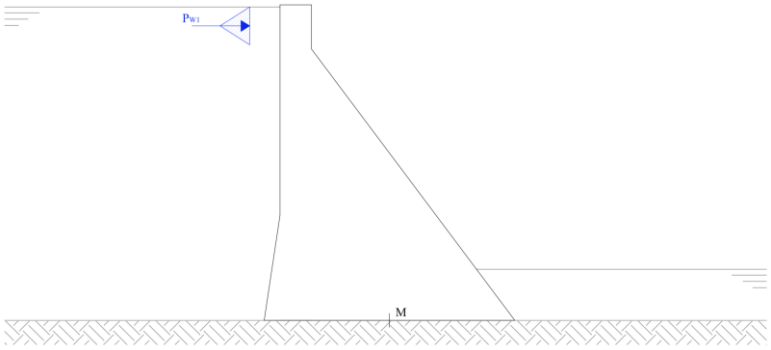

Figure 24. Dynamic water pressure

8.6. Earthquake action

The effects of an earthquake are represented by two forces: the earthquake inertia force on the dam and the seismic dynamic water pressure (figure 25).

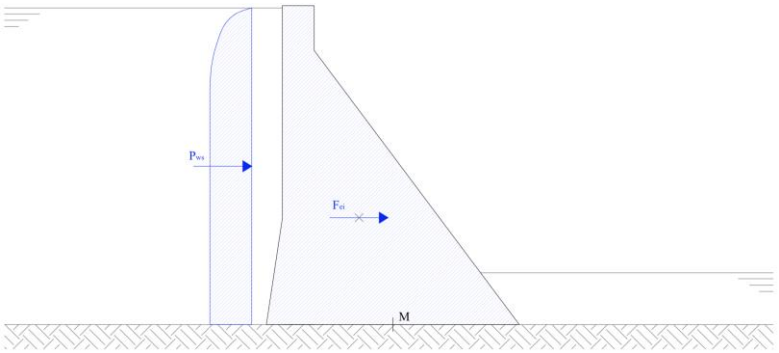

Figure 25. Earthquake inertia force and seismic dynamic water pressure

In order to calculate the earthquake inertia force, the dam is subdivided into ten parts of equal height, see figure 26. Then, the inertia force and the momentum produced by each part is calculated separately as shown in table 8. The horizontal seismic inertia force of part *i* can be calculated with equation 23:

$$F_i = a_h \cdot \xi \cdot G_{ei} \cdot \alpha_i / g \qquad (23)$$

where, a_h is the horizontal earthquake acceleration, equal to ten percent of the gravity acceleration for an earthquake of intensity 7, ξ is the reduction

coefficient of the earthquake action, equal to 0,25 in this project, G_{ei} is the self-weight of the part *i*, α_i is the dynamic distribution coefficient of part *i* and *g* is the gravity acceleration.

The dynamic distribution coefficient for each part is calculated with equation 24 as:

$$\alpha_i = 1.4\frac{1+4(h_i/H)^4}{1+4\sum_{j=1}^{n}\frac{G_{Ej}}{G_E}(h_j/H)^4} \tag{24}$$

where, h_i is the height of part *i*, H is the total height of the dam, G_{ei} is the self-weight of the part *i*, G_e is the self-weight of the dam and *n* is the number of parts.

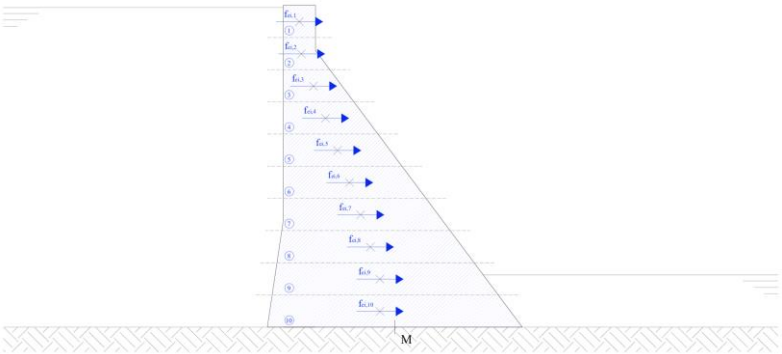

Figure 26. Parts used to compute the earthquake inertia force

Table 8. Calculation of earthquake inertia force and momentum produced by each subdivision or part

Part i	Height h_i (m)	Area A_i (m^2)	Self-weight g_i (kN/m)	$\alpha_{ei,i}$	$f_{ei,i}$	Distance to M $d_{M,i}$	Momentum at M $M_{ei,i}$
1	18,8	353,44	8 482,56	1,40	296,89	178,60	53 024,48
2	18,8	400,76	9 618,25	1,40	336,64	159,80	53 794,87
3	18,8	644,37	15 464,88	1,40	541,27	140,36	75 970,34
4	18,8	909,45	21 826,80	1,40	763,94	121,74	93 004,38
5	18,8	1 174,53	28 188,72	1,40	986,61	103,05	101 666,13
6	18,8	1 439,61	34 550,64	1,40	1 209,27	84,31	101 955,60
7	18,8	1 707,64	40 983,25	1,40	1 434,41	65,56	94 034,97
8	18,8	2 013,95	48 334,80	1,40	1 691,72	46,79	79 154,08
9	18,8	2 332,05	55 969,10	1,40	1 958,92	28,01	54 877,49
10	18,8	2 650,14	63 603,41	1,40	2 226,12	9,23	20 555,72
					11 445,78		728 038,06

The resultant total horizontal force is equal to 11 445,78 kN/m and the momentum produced is 728 038,06 kNm/m.

The action of the waves produced by the earthquake is quantified with equation 25:

$$P_{sw} = 0{,}65 \cdot a_h \cdot \xi \cdot \rho_w \cdot H^2 \qquad (25)$$

where, a_h is the horizontal earthquake acceleration, equal to ten percent of the gravity acceleration for an earthquake of intensity 7, ξ is the reduction coefficient of the earthquake action, equal to 0,25 in this projects, ρ_w is the water density and H is the water elevation upstream of the dam, equal to NWL in this case.

The action point of this force is located 0,54H below the water surface. The value of the seismic dynamic pressure acting on the dam is equal to 5 257,19 kN/m and the momentum produced is 439 165,02 kNm/m.

9. Load combination cases

Application of the partial coefficient method to combine the action of the forces on the dam under two flood conditions: NWL and CWL.

9.1. Partial coefficient method

The Chinese Standard GB50199-2013 "*Unified Design Standard for Reliability of Hydraulic Engineering Structures*" classifies the design situations as: permanent, temporary and accidental. In these design situations, relevant limit states must not be exceeded. These limits states are: ultimate limit state (ULS) and serviceability limit state (SLS). Following this, the effects of the loads are combined with partial coefficients based on the limit state that is being studied in each design situation. The combined effect of the loads shall be lower than the resistance capacity of the material, as shown in equation 26a and 26b:

$$\gamma_0 \psi S(\gamma_G G_k, \gamma_Q Q_k, \alpha_k) \leq \frac{1}{\gamma_{d1}} R(\frac{f_k}{\gamma_m}, \alpha_k) \quad (26a)$$

$$\gamma_0 \psi S(\gamma_G G_k, \gamma_Q Q_k, A_k, \alpha_k) \leq \frac{1}{\gamma_{d2}} R(\frac{f_k}{\gamma_m}, \alpha_k) \quad (26b)$$

where γ_0 is the structural importance coefficient, Ψ is the design condition coefficient, S is the action effect function, R is the structural resistance function, γ_G is the sub coefficient of permanent effect, G_K is the characteristic value of permanent action, γ_Q is the sub coefficient of variable effect, Q_K is the characteristic value of variable action; a_K is the characteristic value of geometry parameter in meters, A_K is the characteristic value of accidental action, γ_{d1} is the basic composite structure coefficient, γ_{d2} is the accidental combined structure coefficient, γ_m is the material properties coefficient and f_K is the characteristic value of material properties.

Three possible scenarios of load combinations are considered:

- Scenario 1: The water level in the reservoir is the CWL. No seismic action is taken into account in this case, since the probability of both accidental events happening at the same time is minimal.
- Scenario 2: The water level in the reservoir is the NWL.
- Scenario 3: The water level in the reservoir is the NWL during an earthquake.

The resulting values for the load combination under scenarios 1, 2 and 3 can be seen in tables 9, 10 and 11 respectively. The values for the coefficients as well as equations 26a and 26b are taken from the Chinese Standard *Unified Standard for Reliability Design of Hydraulic Engineering Structures* (GB50199-2013).

9.2. Combination situations

9.2.1. Scenario 1: CWL

During this accidental design situation, equation 26b is applied to compute the effects produced by the loads as shown in table 9 on the next page.

Table 9. Load combination for scenario 1 and load effects on NOF section

Load and partial coefficient Scenario 1 CWL			Standard or characteristic value (kN/m)				Design value (kN/m)				Force arm (clockwise positive)	Mr (kN·m/m)	Md (kN·m/m)
			Vertical force		Horizontal force		Vertical force		Horizontal force				
			↑	↓	→	←	↑	↓	→	←			
Dam self-weight	G_1	1.0		7 068.80				7 068.80			-68.45	-483 829.91	-483 829.91
	G_2	1.0		84 825.60				84 825.60			-55.91	-4 742 811.36	-4 742 811.36
	G_3	1.0		235 128.01				235 128.01			-6.10	-1 435 260.56	-1 435 260.56
Hydrostatic pressure	P_1	1.0			170 973.05				170 973.05		62.23	10 640 222.53	10 640 222.53
	P_2	1.0				4 562.88				4 562.88	-10.17	-46 389.24	-46 389.24
	P_3	1.0		14 326.98				14 326.98			-69.70	-998 541.13	-998 541.13
	P_4	1.0		3 422.16				3 422.16			59.46	203 490.02	203 490.02
Dynamic water pressure	P_{w1}	1.2			0.13				0.16		186.59	24.49	29.39
Silt pressure	P_{s1}	1.2			21 697.41				26 036.90		30.87	669 726.80	803 672.16
	P_{s2}	1.2		7 717.28				9 260.74			-65.45	-505 115.53	-606 138.64
Uplift pressure	U_1	1.1	7 642.16				8 406.38				70.42	538 176.06	591 993.66
	U_2	1.1	36 391.61				40 030.77				9.48	345 017.69	379 519.46
	U_3	1.1	1 696.45				1 866.09				-70.82	-120 148.53	-132 163.39
Resultant force			45 730.22	352 488.83	192 670.59	4 562.88	50 303.24	354 032.29	197 010.10	4 562.88		4 064 561.33	4 173 793.00

9.2.2. Scenario 2: NWL

Equation 26a is applied to calculate the effects of the loads during the permanent design situation under normal working conditions. Table 10 shows the characteristic and design values of the loads and their effects on the NOF section during scenario 2.

Table 10. Load combination for scenario 2 and load effects on NOF section

Load and partial coefficient Scenario 2 NWL			Standard or characteristic value (kN/m)				Design value (kN/m)				Force arm (clockwise positive)	Mᵢ (kN·m/m)	Mᵈ (kN·m/m)
			Vertical force ↑		Horizontal force →	Horizontal force ←	Vertical force ↑		Horizontal force →	Horizontal force ←			
Dam self-weight	G_1	1.0		7 068.80				7 068.80			-68.45	-483 829.91	-483 829.91
	G_2	1.0		84 825.60				84 825.60			-55.91	-4 742 811.36	-4 742 811.36
	G_3	1.0		235 128.01				235 128.01			-6.10	-1 435 260.56	-1 435 260.56
Hydrostatic pressure	P_1	1.0			161 759.84				161 759.84		60.53	9 791 862.12	9 791 862.12
	P_2	1.0				4 562.88				4 562.88	-10.17	-46 389.24	-46 389.24
	P_3	1.0		13 856.69				13 856.69			-69.70	-965 763.44	-965 763.44
	P_4	1.0		3 422.16				3 422.16			59.46	203 490.02	203 490.02
Dynamic water pressure	P_{w1}	1.2			0.41				0.49		181.37	73.79	88.55
Silt pressure	P_{s1}	1.2			21 697.41				26 036.90		30.87	669 726.80	803 672.16
	P_{s2}	1.2		7 717.28				9 260.74			-65.45	-505 115.53	-606 138.64
Uplift pressure	U_1	1.1	7 433.68				8 177.04				70.43	523 588.86	575 947.75
	U_2	1.1	35 666.45				39 233.10				9.22	328 908.35	361 799.18
	U_3	1.1	1 692.35				1 861.58				-70.82	-119 858.04	-131 843.85
Resultant force			44 792.47	352 018.54	183 457.66	4 562.88	49 271.72	353 562.00	187 797.22	4 562.88		3 218 621.86	3 324 822.79

9.2.3. Scenario 3: NWL and earthquake

The second possible accidental situation studied is the effect of an earthquake during NWL in the reservoir. Results after applying equation 26b are shown in table 11.

Table 11. Load combination for scenario 3 and load effects on NOF section

Load and partial coefficient Scenario 3 NWL + Earthquake			Standard or characteristic value (kN/m)				Design value (kN/m)				Force arm (clockwise positive)	M_R (kN·m/m)	M_d (kN·m/m)
			Vertical force		Horizontal force		Vertical force		Horizontal force				
			↑	↓	→	←	↑	↓	→	←			
Dam self-weight	G_1	1.0		7 068.80				7 068.80			-68.45	-483 829.91	-483 829.91
	G_2	1.0		84 825.60				84 825.60			-55.91	-4 742 811.36	-4 742 811.36
	G_3	1.0		235 128.01				235 128.01			-6.10	1 435 260.56	-1 435 260.56
Hydrostatic pressure	P_1	1.0			161 759.84				161 759.84		60.53	9 791 862.12	9 791 862.12
	P_2	1.0				4 562.88				4 562.88	-10.17	-46 389.24	-46 389.24
	P_3	1.0		13 856.69				13 856.69			-69.70	-965 763.44	-965 763.44
	P_4	1.0		3 422.16				3 422.16			59.46	203 490.02	203 490.02
Dynamic water pressure	P_{w1}	1.2			0.41				0.49		181.37	73.79	88.55
Silt pressure	P_{s1}	1.2			21 697.41				26 036.90		30.87	669 726.80	803 672.16
	P_{s2}	1.2		7 717.28				9 260.74			-65.45	-505 115.53	-606 138.64
Uplift pressure	U_1	1.1	7 433.68				8 177.04				70.43	523 588.86	575 947.75
	U_2	1.1	35 666.45				39 233.10				9.22	328 908.35	361 799.18
	U_3	1.1	1 692.35				1 861.58				-70.82	-119 858.04	-131 843.85
Earthquake inertia force	F_e	1.0			11 445.78				11 445.78				
Seismic dynamic water pressure	P_{ws}	1.0			5 257.19				5 257.19		83.54	439 165.02	439 165.02
Resultant force			44 792.47	352 018.54	200 160.64	4 562.88	49 271.72	353 562.00	204 500.20	4 562.88		3 657 786.87	3 763 987.80

10. Stability analysis

Study of overturning, sliding, seepage and compressive capacity at the body-foundation interface under NWL and CWL conditions. The texts "Hydraulic Structures" by Novak et al. (2007) and "Design of Small Dams" by USBR (1987) are followed to perform the stability analysis.

The stability of the dam is studied in the most vulnerable section of the dam. The central section of the dam, marked as S1 in figure 27, is the largest section of the structure, thus the one withstanding the largest forces. The NOF section S1 is located 371,74 meters from the left abutment. This section is analysed under the load combination cases defined in chapter 8.

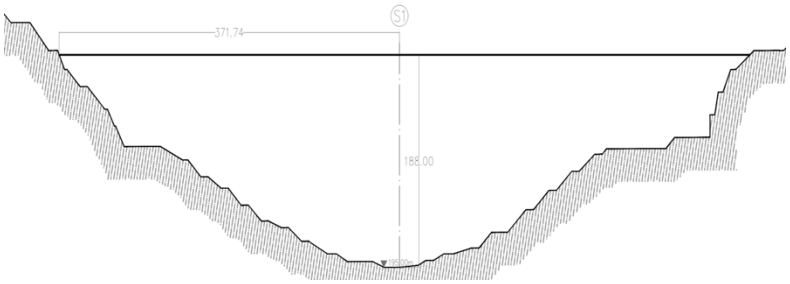

Figure 27. Cross-section S1

It is assumed that the dam is formed by vertical elements that individually carry their load to the rock foundation without any load transfer from or to adjacent elements. It is also assumed that the vertical stresses follow a linear variation from upstream to downstream on all horizontal sections. Having these assumptions in consideration, in order for the dam to be stable, it shall be safe against sliding, overturning and the safe unit stresses in the concrete shall not be exceeded (Novak et al., 2007).

10.1. Overturning

Scenario 3 is excluded from the overturning analyses, due to the transient and oscillatory nature of the seismic loads. To estimate the probability of overturning, the moments produced at the toe by all the loads acting on the dam are computed and contrasted. Following the sign convention diagram in figure 18, are considered restoring moments those that produce a positive moment at the toe, and overturning moments, those that produce a negative moment. The safety factor against overturning f_O, is the proportion of restoring moments against overturning ones. This factor should be over 1,5 though a value up to 1,25 is still considered acceptable. There is risk of failure due to overturning with safety factors lower than 1,25 (Novak et al., 2007).

Table 12. Study of overturning risk under CWL conditions in section S1

Load	Symbol	Units	Value	Distance to TOE	Moment at TOE
Self-weight concrete					
SW1	g_{c1}	kN/m	7 068,80	143,16	1 011 957,63
SW2	g_{c2}	kN/m	84 825,60	130,63	11 080 344,00
SW3	g_{c3}	kN/m	235 128,01	80,82	19 002 262,01
Hydrostatic pressure					
Horizontal 1	p_{H1}	kN/m	170 973,05	-62,23	-10 640 222,53
Horizontal 2	p_{H2}	kN/m	4 562,88	10,17	46 389,24
Vertical 1	P_{v1}	kN/m	14 326,98	144,41	2 068 945,76
Vertical 2	P_{v2}	kN/m	3 422,16	7,63	26 093,95
Uplift					
Uplift 1	u_1	kN/m	7 642,16	-145,13	-1 109 141,31
Uplift 2	u2	kN/m	36 391,61	-84,19	-3 063 925,58
Uplift 3	u3	kN/m	1 696,45	-3,89	-6 597,30
Dynamic water pressure					
Horizontal 1	p_{w1}	kN/m	0,13	-186,81	-24,52
Silt pressure					
Horizontal 1	p_{sH}	kN/m	21 697,41	-30,87	-669 726,80
Vertical 1	p_{sV}	kN/m	7 717,28	140,17	1 081 693,11

Restoring moments	+M		34 317 685,70
Overturning moments	-M		15 483 016,22
Safety factor againt overturning	F_O	2,2	OK

Table 13. Study of overturning risk under NWL conditions in section S1

Load	Symbol	Units	Value	Distance to TOE	Moment at TOE
Self-weight concrete					
SW1	g_{c1}	kN/m	7 068,80	143,16	1 011 957,63
SW2	g_{c2}	kN/m	84 825,60	130,63	11 080 344,00
SW3	g_{c3}	kN/m	235 128,01	80,82	19 002 262,01
Hydrostatic pressure					
Horizontal 1	p_{H1}	kN/m	161 759,84	-60,53	-9 791 862,12
Horizontal 2	p_{H2}	kN/m	4 562,88	10,17	46 389,24
Vertical 1	P_{v1}	kN/m	13 856,69	144,41	2 000 882,84
Vertical 2	P_{v2}	kN/m	3 422,16	7,63	26 093,95
Uplift					
Uplift 1	u_1	kN/m	7 433,68	-145,14	-1 078 947,85
Uplift 2	u2	kN/m	35 666,45	-83,93	-2 993 638,06
Uplift 3	u3	kN/m	1 692,35	-3,89	-6 581,34
Dynamic water pressure					
Horizontal 1	p_{w1}	kN/m	0,41	-181,71	-73,93
Silt pressure					
Horizontal 1	p_{sH}	kN/m	21 697,41	-30,87	-669 726,80
Vertical 1	p_{sV}	kN/m	7 717,28	140,17	1 081 693,11

Restoring moments	+M		34 249 622,77
Overturning moments	-M		14 534 174,84
Safety factor againt overturning	F_O	2,4	OK

Studying section S1 the safety factor is 2,2 under CWL conditions, and 2,4 under NWL. As seen in tables 12 and 13, there is no overturning hazard present in neither NWL nor CWL situation.

10.2. Sliding

Generally, the condition of safety against sliding has to be met in three areas of the dam: in the dam body, especially horizontal construction joints, in the dam-foundation interface, and in the foundation, especially in geological discontinuities and fractures. Only the second one is studied in this preliminary design. The influence of joints and the of the fractures and discontinuities in the foundation would require a more in detailed study that exceeds the scope of the present report.

The stability of the dam against sliding is measured with the homonymous factor, that in this case is estimated as the shear friction factor F_{SF} shown in equation 27a (Novak et al., 2007).

$$F_{SF} = \frac{S}{\sum H} \quad (27a)$$

where S is the maximum shear resistance that can be mobilised on a plane, calculated with equation 27b, and H is the total horizontal load in kilonewton.

$$S = c \cdot A_h + \sum V \cdot tan\phi \quad (27a)$$

where c is the cohesion in meganewton per square meter, A_h is the area of plane of contact or thickness in 2D in square meter, V is the total vertical load in kilonewton and ϕ is the angle of shearing resistance.

Recommended values for c and $tan\phi$ at the concrete-rock interface for sound rock are 1,0-3,0 MNm^{-2} and 1,0-1,8 respectively (USBR, 1987). Tables 14, 15 and 16 include the selected values for the present design, these being selected as 1,5 MNm^{-2} and 1,1 respectively.

The USBR (1987) recommends that the minimum F_{SF} at the concrete-rock interface should be 3,0 for scenario 2 and greater than 1,0 for scenarios 1 and 3. Following this, the present design is at risk of sliding in scenario 2 (tables 15a and 15b). This does not come as a surprise since the condition of safety against sliding is usually the most critical of all the conditions that need to be met by the design (Novak et al., 2007). As the resultant vertical load $\sum V$ is several orders of magnitude larger than the thickness of the dam, this value is most influential on the shear resistance. Consequently, the selection of a larger or smaller $tan\phi$ strongly affects the resistance capacity against sliding (tables 15a and 15b). Measures that shall be taken to ensure safety against sliding are:

- Reducing uplift pressure.
- Increasing self-weight.
- Reducing to a minimum the silt pressure.

Table 14. Study of sliding risk under CWL conditions in section S1

Load	Symbol	Unit	Value	
Shear friction factor	F_{SF}		1,74	**OK**
Area of plane of contact or sliding	A_h	m^2	149,43	
Cohesion	c	MN/m^2	1,5	
Normal actions at dam-rock interface	ΣV	kN	303 729,05	
Frictional resistance to shearing	tanø		1,1	
Tangential actions at base of dam	ΣH		192 447,20	

Table 15a. Study of sliding risk under NWL conditions in section S1

Load	Symbol	Unit	Value	
Shear friction factor	F_{SF}		1,83	Sliding hazard
Area of plane of contact or sliding	A_h	m^2	149,43	
Cohesion	c	MN/m^2	1,5	
Normal actions at dam-rock interface	ΣV	kN	304 290,28	
Frictional resistance to shearing	tanø		1,1	
Tangential actions at base of dam	ΣH		183 234,28	

Table 15b. Study of sliding risk under NWL conditions in section S1 with larger tanϕ

Load	Symbol	Unit	Value	
Shear friction factor	F_{SF}		2,16	Sliding hazard
Area of plane of contact or sliding	A_h	m^2	149,43	
Cohesion	c	MN/m^2	1,5	
Normal actions at dam-rock interface	ΣV	kN	304 290,28	
Frictional resistance to shearing	tanø		1,3	
Tangential actions at base of dam	ΣH		183 234,34	

Table 16. Study of sliding risk under NWL and earthquake conditions in section S1

Load	Symbol	Unit	Value	
Shear friction factor	F_{SF}		1,68	**OK**
Area of plane of contact or sliding	A_h	m^2	149,43	
Cohesion	c	MN/m^2	1,5	
Normal actions at dam-rock interface	ΣV	kN	304 290,28	
Frictional resistance to shearing	tanø		1,1	
Tangential actions at base of dam	ΣH		199 937,32	

10.3. Compressive strength

The normal compressive stresses at the dam-rock interface are computed with equation 28. The vertical stresses are calculated at the upstream and downstream walls, and a linear variation between them is assumed, figure 28.

$$\sigma_z = \frac{\Sigma V}{T}(1 \pm \frac{6e}{T}) \quad (28)$$

where T is the dam thickness, V is the resultant vertical load on the horizontal plane and e is the eccentricity of the resultant vertical load.

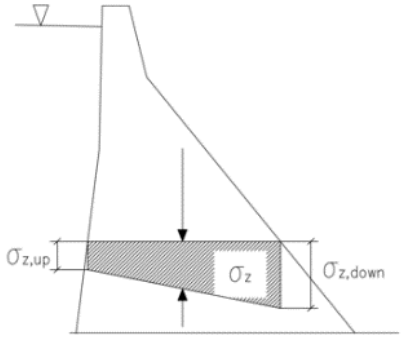

Figure 28. Vertical normal stresses on horizontal planes, σ_z

The previous equation is applied in tables 17 and 18 for scenarios 1 and 2 respectively, showing that there are no tensile stresses developed and the compressive capacity of the material, concrete is not surpassed. Given there is no vertical component of the earthquake action, this scenario is equal to NWL.

Table 17. Vertical normal stresses under CWL conditions in section S1 at concrete-rock interface

Load	Symbol	Unit	Value		
Vertical normal stress upstream	$\sigma_{z,up}$	kN/m^2	1 473,26		OK
Vertical normal stress downstream	$\sigma_{z,down}$	kN/m^2	3 265,34		OK
Thickness	T	m	149,4		
Resultant vertical load above plane	ΣV	kN	354 032,29		
Eccentricity of resultant load	e	m	9,4	49,8	OK
Moments at centroid of plane (O)	ΣM*	kNm	3 334 439,59		

Table 18. Vertical normal stresses under NWL conditions in section S1 at concrete-rock interface

Load	Symbol	Unit	Value	
Vertical normal stress upstream	$\sigma_{z,up}$	kN/m^2	1 571,25	
Vertical normal stress downstream	$\sigma_{z,down}$	kN/m^2	3 161,05	
Thickness	T	m	149,4	
Resultant vertical load above plane	ΣV	kN	353 562,00	
Eccentricity of resultant load	e	m	8,4	49,8
Moments at centroid of plane (O)	ΣM*	kNm	2 958 073,66	

10.3.1. Middle third rule

In order for the structure to be stable and no tensions to be developed between the dam and the foundation, the resultant of the vertical load shall fall within the middle third area of the total surface as shown in figure 29.

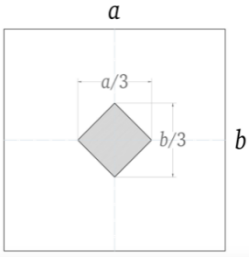

Figure 29. Middle-third rule

The thickness of the dam is 149,4 meters at the body-foundation interface. This means that the resultant vertical load shall be within the central 49,8 meters. Dividing the moment produced at M by the value of the resultant load, the eccentricity of the resultant load is 9,4 meters. Therefore, no tensions are developed at the base of the dam.

10.4. Seepage analysis with GeoStudio

The seepage analysis was conducted for steady-state conditions by using the SEEP/W software in GeoStudio. The calculations performed in SEEP/W are based on Darcy's law (GEO-SLOPE Intl. Ltd., 2012). The coordinate system follows the one defined in figure 18.

The following points were studied in the seepage analysis with GeoStudio:

- Velocity field
- Pore-water pressure
- Pressure head
- Flow net
- Seepage velocity (Y- and Z-direction)

The analysis was performed for the S1 cross-section, where the dam has the largest dimensions, see figure 27. The structure was analysed under both NWL and CWL conditions. The material properties used for the seepage analysis can be seen in table 19.

Table 19. List of material properties used in the seepage analysis

Material	Colour in FE-model	Hydraulic conductivity, K_{hx} (m/s)	Matric suction (KPa)	Material model
R-1 (Concrete)		$1{,}7 \cdot 10^{-12}$	0,001	Saturated/ Unsaturated
R-2 (RCC)		$2{,}7 \cdot 10^{-12}$	0,001	Saturated/ Unsaturated
Grout curtain		$1{,}6 \cdot 10^{-12}$	0,001	Saturated/ Unsaturated
Base (Limestone)		$4.9 \cdot 10^{-7}$	0,001	Saturated/ Unsaturated

The material model was set as *Saturated/Unsaturated* because the water content in the materials is unknown, and SEEP/W asks for the water content when modelling saturated materials. Instead, the matric suction (matric potential) was set to almost zero (0,001 kPa) for every material because that corresponds to saturated conditions (SoilSensor, n.d.). This assumption should be suitable for the circumstances that are modelled because most of the materials are submerged under the reservoir water or tailwater.

The foundation at the dam site consists of a thick layer of limestone, which is why the hydraulic conductivity for limestone found in Linsley et al. (1992) was set as the hydraulic conductivity for the base material. The hydraulic conductivity for the upstream face concrete wall and the RCC was based on experimental results found in Mesic et al. (1994). Test results of the hydraulic conductivity for a mix incorporating standard Portland cement was used for the concrete, and test results from a mixture with standard Portland cement and fly ash was used as the value for the RCC. The hydraulic conductivity for a cement-based grout mix found in Allan and Philippacopoulos (1999) was used as the value for the grout curtain. It was assumed that all materials are isotropic. The model that was used for the seepage analysis can be seen in figure 30.

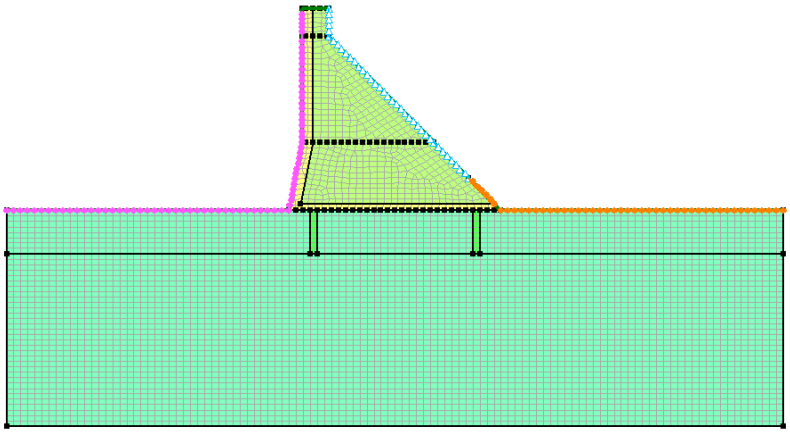

Figure 30. FE-model of the dam that was used in the seepage analysis

According to the Chinese Standard DL5108-1999, the upstream curtain must be located 0.1 times the length of the base of the dam from the dam heel, while the downstream curtain can be located arbitrarily. Furthermore, the standard says that the upstream curtain must be at least 40 meters long and 5 meters thick. The curtains seen in figure 30 are located 15 meters from either the heel or the toe of the dam respectively, they are 40 meters deep and 5 meters thick. The boundary conditions (pink, orange and blue colour in figure 30) can be seen in table 20. The upstream boundary was set as either the NWL (181,6 meters) or CWL (186,7 meters). The tailwater level was set as 30,5 meters.

Table 20. Boundary conditions applied to the FE-model in the seepage analysis

Boundary	Colour	Type	Head (m)	Total flux (m^3/s)
Upstream		Head	NWL or CWL	-
Downstream		Head	TWL	-
Potential Seepage Face		Total Flux	-	0

10.4.1. Results

Seepage – Velocity field – NWL conditions

In figure 31 the seepage velocity field during NWL conditions can be seen. The black arrows represent the seepage velocity, where the longer arrows correspond to a higher seepage velocity. The highest flow of water occurs under the curtains and at the heel and toe of the dam, while the seepage directly under the dam is lower.

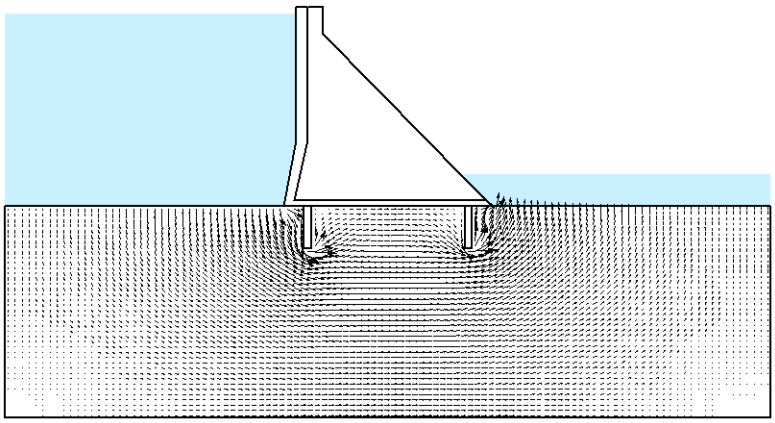

Figure 31. Seepage velocity field during NWL conditions

Seepage – Pore-water pressure – NWL conditions

The pore-water pressure during NWL conditions can be seen in figure 32. The colour scale on the left side in figure 32 shows the pressure that each colour in the figure represents. The pore-water pressure has a value of 1 000-1 500 kPa between the curtains underneath the base of the dam.

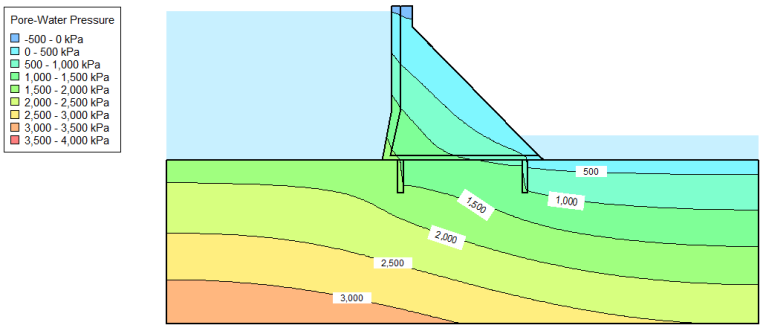

Figure 32. The pore-water pressure during NWL conditions

Seepage – Pressure head (with flow net) – NWL conditions

Figure 33 shows the pressure head as well as the flow net during NWL conditions. The flow net is represented with the green lines. The effect of the curtains can be seen by studying the flow net between the curtains and the equipotential lines of the pressure head. It can be seen that the flow directly underneath the base of the dam is reduced with the grout curtains. The colour scale on the left side in figure 33 shows the total head that each colour in the figure represents. The pressure head is 181,6 meters (NWL) upstream and 30,5 meters downstream (TWL).

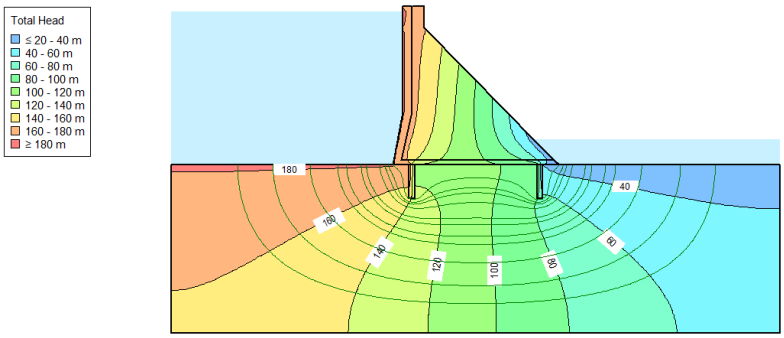

Figure 33. Pressure head and flow net (green lines) during NWL conditions

Seepage in Y-direction – NWL conditions

Figure 34 shows that the seepage velocity in the Y-direction during NWL conditions. The colour scale on the left side in figure 34 shows the velocity that each colour in the figure represents. The peak value is $5{,}0 \cdot 10^{-7}$ m/s which occurs underneath the grout curtains.

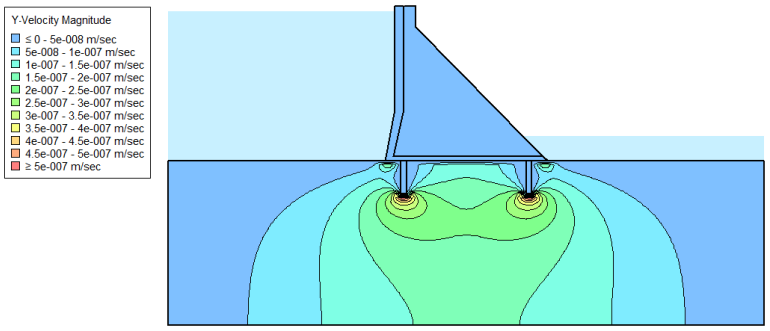

Figure 34. Seepage velocity in the Y-direction during NWL conditions

Seepage in Z-direction – NWL conditions

Figure 35 shows that the seepage velocity in the Z-direction during NWL conditions. The colour scale on the left side in figure 35 shows the velocity that each colour in the figure represents. The peak value is $4{,}5 \cdot 10^{-7}$ m/s which occurs next to the dam heel, curtains and the dam toe.

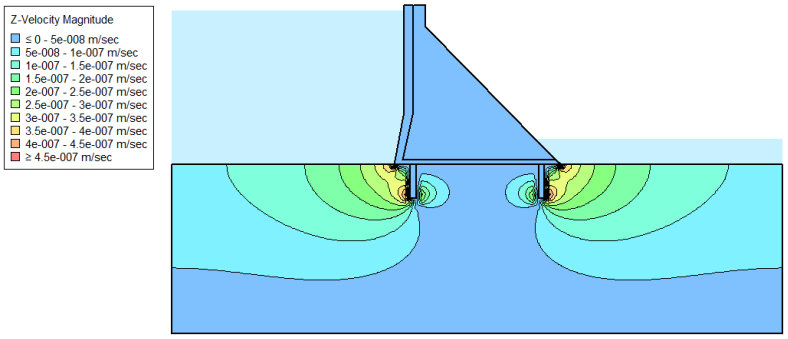

Figure 35. Seepage velocity in the Z-direction during NWL conditions

Seepage – Velocity field – CWL conditions

In figure 36 the seepage velocity field during CWL conditions can be seen. The black arrows represent the seepage velocity, where the longer arrows correspond to a higher seepage velocity. The highest flow of water occurs under the curtains and at the heel and toe of the dam, while the seepage directly under the dam is lower.

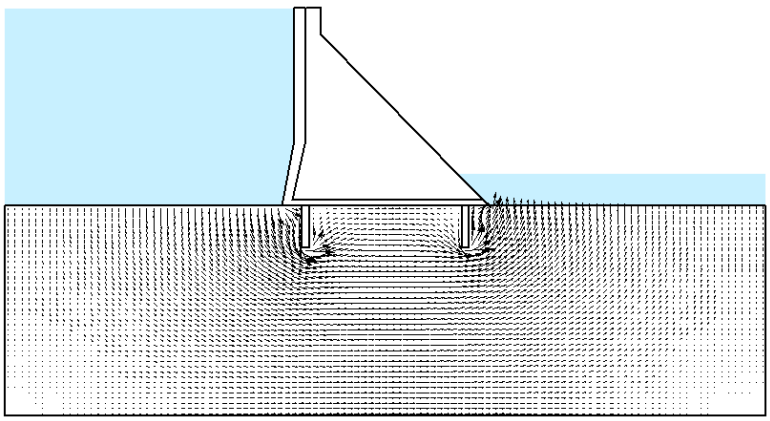

Figure 36. Seepage velocity field during CWL conditions

Seepage – Pore-water pressure – CWL conditions

The pore-water pressure during CWL conditions can be seen in figure 37. The colour scale on the left side in figure 37 shows the pressure that each colour in the figure represents. The pore-water pressure has a value of 1 000-1 500 kPa between the curtains underneath the base of the dam.

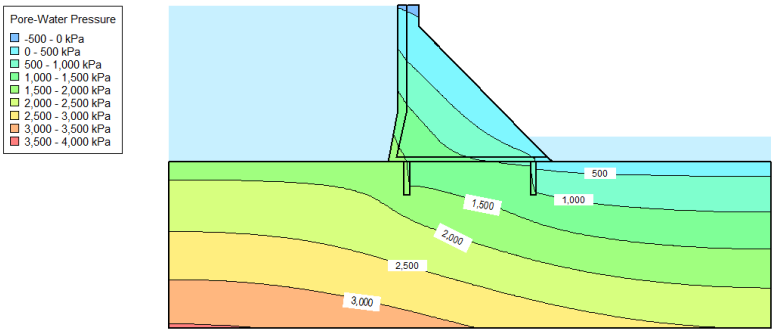

Figure 37. The pore-water pressure during CWL conditions

Seepage – Pressure head (with flow net) – CWL conditions

Figure 38 shows the pressure head as well as the flow net during CWL conditions. The flow net is represented with the green lines. The effect of the curtains can be seen by studying the flow net between the curtains and the equipotential lines of the pressure head. It can be seen that the flow directly underneath the base of the dam is reduced with the grout curtains. The colour scale on the left side in figure 38 shows the total head that each colour in the figure represents. The pressure head is 181,6 meters (NWL) upstream and 30,5 meters downstream (TWL).

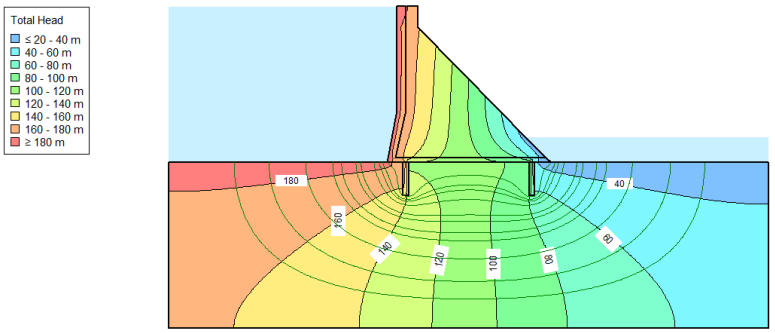

Figure 38. Pressure head with flow net (green lines) during CWL conditions

Seepage in Y-direction – CWL conditions

Figure 39 shows that the seepage velocity in the Y-direction during CWL conditions. The colour scale on the left side in figure 39 shows the velocity that each colour in the figure represents. The peak value is $5{,}0 \cdot 10^{-7}$ m/s which occurs underneath the grout curtains.

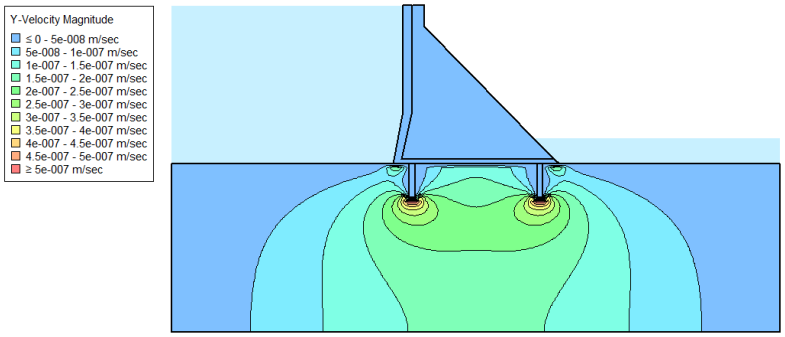

Figure 39. Seepage velocity in the Y-direction during CWL conditions

Seepage in Z-direction – CWL conditions

Figure 40 shows that the seepage velocity in the Z-direction during CWL conditions. The colour scale on the left side in figure 40 shows the velocity that each colour in the figure represents. The peak value is $4{,}5 \cdot 10^{-7}$ m/s which occurs next to the dam heel, curtains and dam toe.

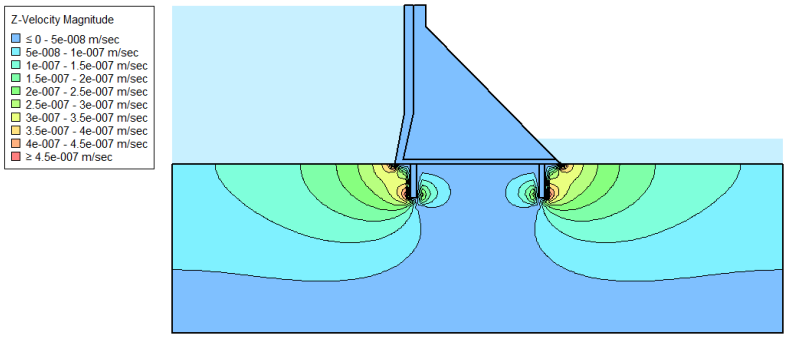

Figure 40. Seepage velocity in the Z-direction during CWL conditions

10.4.2. Discussion

The seepage results from SEEP/W during both NWL conditions and CWL conditions are very similar and no significant difference can be observed between the two cases.

The velocity fields in figure 31 and figure 36 show that the highest velocities occur underneath the dam heel, grout curtains and the dam toe while the seepage underneath the dam base is smaller. The flow nets in figure 33 and figure 38 reveal that the seepage flow underneath the base of the dam is reduced by the grouting curtains. This can also be seen in figure 39 and figure 40 where the seepage velocity in the area between the grout curtains is lower than in the surrounding area. There is also a significant drop in the pore-water pressure that can be observed at the curtains in figure 32 and figure 37. The pore-water pressure is reduced from 2 000 kPa to 1 500 kPa at the upstream curtain and from 1 500 kPa to 1 000 kPa at the downstream curtain. This implies that the grout curtains work as intended.

The highest seepage velocity in the Y-direction is $5{,}0 \cdot 10^{-7}$ m/s and $4{,}5 \cdot 10^{-7}$ m/s in the Z-direction (figure 39 and figure 40). These are small values, which shouldn't lead to any complications even though some of the highest seepage velocities occur next to sensitive regions like the heel and toe. The limit for seepage velocities that might induce harmful scour and erosion in loose earth and rocks is 0,6-1,0 m/s (Linsley et al., 1992).

11. Stress analysis

Stress analysis at the horizontal plane defined by the concrete-rock interface during NWL, CWL and earthquake conditions. Study of shear and principal stresses applying the gravity method. Results are compared to permissible stresses of concrete. The texts "Hydraulic Structures" by Novak et al. (2007) and "Design of Small Dams" by USBR (1987) are followed to perform the stress analysis.

11.1. Gravity method

By gravity method, stress analysis is performed for a unit dam slice perpendicular to the dam axis, that is, a "planar problem". Stress calculations are made for a non-overflow dam monolith, in which the positive directions of coordinate axes, loads, and stresses follow the sign convention previously shown in figure 18. The stresses of up- and downstream faces are indicated by the superscript "up" and "down", respectively.

11.2. Shear stresses

Variations in vertical normal stresses over a horizontal plane at any point, generate shear stresses. These are computed at the upstream (equation 29a) and downstream (equation 29b) faces and a parabolic variation is assumed between them (figure 41).

$$\tau_{zy,up} = (p_w - \sigma_{z,up}) tan\phi_{up} \quad (29a)$$

$$\tau_{zy,down} = \sigma_{z,down} tan\phi_{down} \quad (29b)$$

where p_w is the hydrostatic pressure in kilonewton per meter, $tan\phi$ is the slope of the upstream and downstream walls and σ_z is the vertical normal stress at the upstream and downstream walls. The computed values of the shear stresses for scenarios 1, 2 and 3 are presented in tables 21, 22 and 23 respectively.

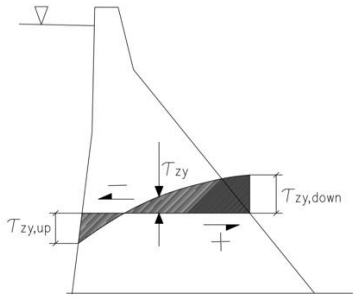

Figure 41. Shear stresses on horizontal planes, τ_{zy}

Table 21. Shear stresses under CWL conditions in section S1 at concrete-rock interface

Load	Symbol	Unit	Value		
Horizontal shear stress upstream	$\tau_{xy,up}$	kN/m^2	53,74		OK
Horizontal shear stress downstream	$\tau_{xy,down}$	kN/m^2	2 449,00		OK
Hydrostatic pressure upstream	P_1	kN/m	1 831,53		
Vertical normal stress upstream	$\sigma_{z,up}$	kN/m^2	1 473,26		
Vertical normal stress downstream	$\sigma_{z,down}$	kN/m^2	3 265,34		
Slope upstream	n		0,15		
Slope downstream	m		0,75		

Table 22. Shear stresses under NWL conditions in section S1 at concrete-rock interface

Load	Symbol	Unit	Value		
Horizontal shear stress upstream	$\tau_{xy,up}$	kN/m^2	31,54		OK
Horizontal shear stress downstream	$\tau_{xy,down}$	kN/m^2	2 370,79		OK
Hydrostatic pressure upstream	P_1	kN/m	1 781,50		
Vertical normal stress upstream	$\sigma_{z,up}$	kN/m^2	1 571,25		
Vertical normal stress downstream	$\sigma_{z,down}$	kN/m^2	3 161,06		
Slope upstream	n		0,15		
Slope downstream	m		0,75		

Table 23. Shear stresses under NWL + earthquake conditions in section S1 at concrete-rock interface

Load	Symbol	Unit	Value		
Horizontal shear stress upstream	$\tau_{xy,up}$	kN/m^2	365,46		OK
Horizontal shear stress downstream	$\tau_{xy,down}$	kN/m^2	2 370,79		OK
Hydrostatic pressure upstream	P_1	kN/m	1 781,50		
Horizontal earthquake inertia force	f_{ei}		2 226,10		
Vertical normal stress upstream	$\sigma_{z,up}$	kN/m^2	1 571,25		
Vertical normal stress downstream	$\sigma_{z,down}$	kN/m^2	3 161,06		
Slope upstream	n		0,15		
Slope downstream	m		0,75		

11.3. Principal stresses

Equations 30a and 30b are used to calculate the maximum and minimum principal stress respectively, illustrated in figure 42.

$$\sigma_1 = \frac{\sigma_z+\sigma_y}{2} + \tau_{max} \tag{30a}$$

$$\sigma_3 = \frac{\sigma_z+\sigma_y}{2} - \tau_{max} \tag{30b}$$

where σ_z is the vertical normal stress, σ_y is the horizontal normal stress and τ_{max} is the maximum shear stress that can be computed with equation 31:

$$\tau_{max} = \left(\left(\frac{\sigma_z-\sigma_y}{2}\right)^2 + \tau^2\right)^{1/2} \tag{31}$$

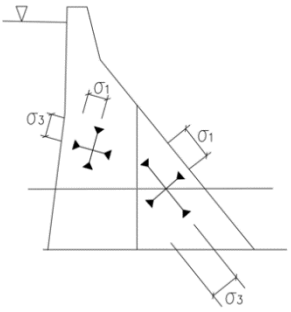

Figure 42. Principal stresses, σ_1 and σ_3

The maximum and minimum principal stresses occur at the upstream and downstream dam faces, since they are both planes of zero shear stresses. The boundary values σ_1 and σ_3 are calculated with equations 32a and 32b for the upstream face and 32c and 32d for the downstream face.

$$\sigma_{1,up} = \sigma_{z,up}\left(1 + tan^2\phi_{up}\right) - p_w tan^2\phi_{up} \tag{32a}$$

$$\sigma_{3,up} = p_w \tag{32b}$$

$$\sigma_{1,down} = \sigma_{z,down}(1 + tan^2\phi_{down}) \quad (32c)$$

$$\sigma_{3,down} = 0 \quad (32d)$$

where $\sigma_{z,up}$ and $\sigma_{z,down}$ are the vertical normal stress on the upstream and downstream faces, p_w is the hydrostatic pressure upstream and $tan\phi$ is the slope of the upstream and downstream faces.

The resulted values of the principal stresses for CWL and NWL conditions are shown in tables 24 and 25.

Table 24. Principal stresses under CWL condition in section S1

Load	Symbol	Unit	Value		
Major principal stress upstream	$\sigma_{1,up}$	kN/m^2	1 465,20		OK
Major principal stress upstream	$\sigma_{1,down}$	kN/m^2	5 102,09		OK
Hydrostatic pressure upstream	P_1	kN/m	1 831,53		
Vertical normal stress upstream	$\sigma_{z,up}$	kN/m^2	1 473,26		
Vertical normal stress downstream	$\sigma_{z,down}$	kN/m^2	3 265,34		
Slope upstream	n		0,15		
Slope downstream	m		0,75		

Table 25. Principal stresses under NWL condition in section S1

Load	Symbol	Unit	Value		
Major principal stress upstream	$\sigma_{1,up}$	kN/m^2	1 566,51		OK
Major principal stress upstream	$\sigma_{1,down}$	kN/m^2	4 939,15		OK
Hydrostatic pressure upstream	P_1	kN/m	1 781,50		
Vertical normal stress upstream	$\sigma_{z,up}$	kN/m^2	1 571,25		
Vertical normal stress downstream	$\sigma_{z,down}$	kN/m^2	3 161,06		
Slope upstream	n		0,15		
Slope downstream	m		0,75		

11.4. Permissible stresses

As stated by Novak et al. (2007) the compressive stresses generated in gravity dams are generally very low, seldom exceeding 2,0–3,0 MN/m^2, which is congruent with the results obtained for the present design. Either a safety factor or a maximum allowable compressive stress is defined. The USBR (1987) sets this maximum value as 10 MN/m^2 for NWL condition and as 15 MN/m^2 for CWL condition.

All of the computed stresses are far from these allowable values, making the designed dam qualify as safe. It must be remembered that all normal stresses shall be larger or equal to zero, to prevent the development of tensile stresses.

11.5. Stress analysis with GeoStudio

The SIGMA/W software in GeoStudio was used to conduct a numerical analysis of the stresses and deformations in the structure. The calculations in SIGMA/W are based on either two-dimensional plane strain theory or small displacement- and small strain theory for axisymmetric problems (GEO-SLOPE Intl. Ltd., 2013). Only linear-elastic theory was used in the analysis. Positive stresses denote compression and negative stresses denote tension. The coordinate system used follows the positives defined in figure 18.

The following points were studied in SIGMA/W:

- Deformed grid
- Displacement vector
- Displacements (Y-, Z- and YZ-direction)
- Stresses (Shear, Y- & Z-direction, Maximum, Minimum)

The analysis was performed on the S1 cross-section, where the dam has the largest dimensions, see figure 27. The structure was analysed under both NWL- and CWL conditions.

The material properties for the stress and displacement analysis were set according to table 26.

Table 26. List of material properties used in the stress- and displacement analysis

Material	Colour in model	Young's modulus (GPa)	Unit weight (kN/m^3)	Poisson's ratio
Dam Concrete		20	24	0,2
Grout curtain		14,5	21,4	0,23
Base (Limestone)		20	25	0,3

The material properties for the base were selected based on the fact that the foundation consists of a thick layer of limestone. The Young's modulus for the limestone was found in Graham (1997), the unit weight was found in Fine (n.d.) and the Poisson ratio for limestone was found in Engineering ToolBox (2008a). The material parameters for the grout curtain were selected based on experimental results for a cement-based grout mix found in Allan and Philippacopoulos (1999). A simplification was made, in the sense that is assumed that the whole dam body is constructed with the same concrete material. The unit weight of concrete was assumed to be 24 kN/m^3, while the values for the Young's modulus and Poisson's ratio for concrete were retrieved from Engineering ToolBox (2008b).

The model that was used in the analysis can be seen in figure 43. The base is constrained from moving in the Y- and Z-direction at the bottom and the sides of the base are restrained from moving in the Y-direction (see orange colour). The loads applied in the model are upstream hydrostatic pressure (pink), downstream hydrostatic pressure (light blue), uplift (red) and self-weight. The uplift was applied according to section 8.3.

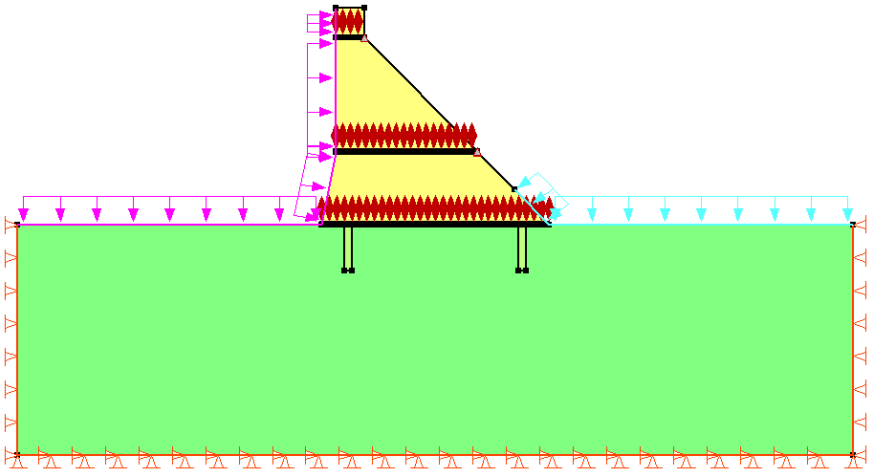

Figure 43. FE-model of the dam that used in the stress- and displacement analysis

11.5.1. Results

Displacements – Deformed grid – NWL conditions

The deformed grid during NWL conditions can be seen in red in figure 44, where the displacements have been magnified with a factor of 350 to make the deformation noticeable. The dam seems to get tilted towards the downstream side and pressured down towards the foundation.

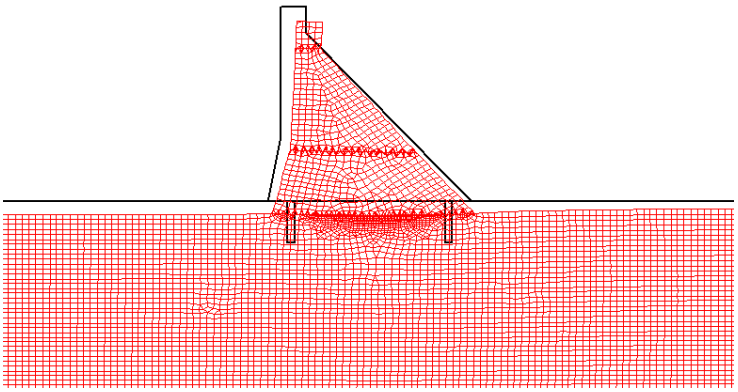

Figure 44. The deformed grid of the dam (magnified with a factor of 350) during NWL conditions

Displacements – Displacement vectors - NWL conditions

The displacement vectors during NWL conditions can be seen in red in figure 45. The vectors show towards which direction each point is going to be displaced. The displacement vectors at the top of the dam body are directed towards the dam toe while the vectors at the dam base are more vertical directed towards the foundation. This should imply that the top of the dam body wants to tilt to the downstream side while the base is pressured to the foundation.

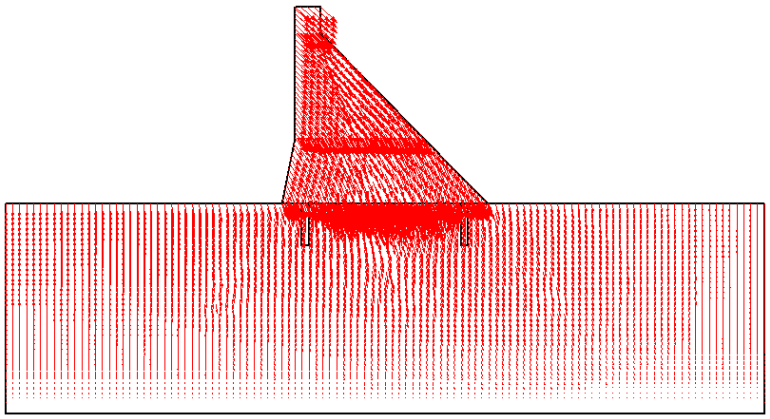

Figure 45. Displacement vectors during NWL conditions

Displacements in Y-direction - NWL conditions

Figure 46 shows the displacements in the Y-direction during NWL conditions. The colour scale on the left side in figure 46 shows what displacement each colour in the figure represents. The top of the structure is tilted 3,2 centimetres to the downstream side. The foundation underneath the base of the dam is displaced around 1,0 centimetres to the downstream side.

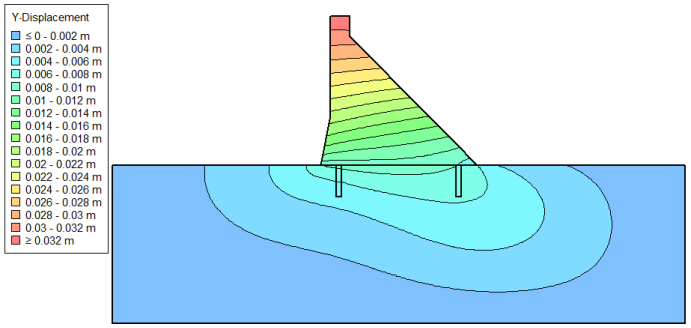

Figure 46. Displacement in the Y-direction during NWL conditions

Displacements in Z-direction - NWL conditions

Figure 47 shows the displacements in the Z-direction during NWL conditions. The colour scale on the left side in figure 47 shows what displacement each colour in the figure represents. The displacement in the dark blue area at the top of the structure is 4,0 centimetres downwards. The foundation underneath the base of the dam is displaced circa 3,0 centimetres downwards.

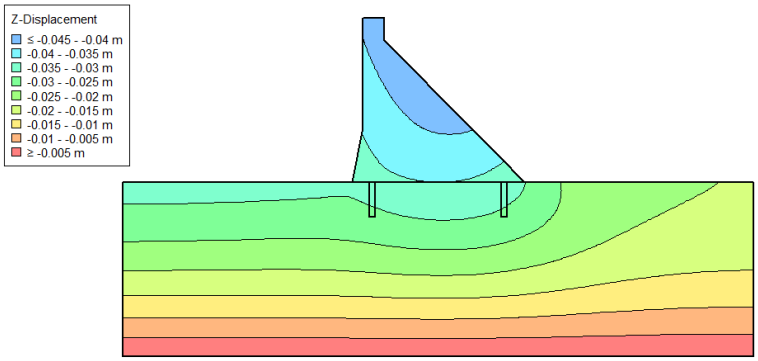

Figure 47. Displacement in the Z-direction during NWL conditions

Displacements in YZ-direction - NWL conditions

The displacement in the YZ-direction during NWL conditions can be seen in figure 48. The colour scale on the left side in figure 48 shows what displacement each colour in the figure represents. The displacement is around 5,0 centimetres in the YZ-direction at the top of the dam. At the foundation underneath the base of the dam the displacement in the YZ-direction is around 4,0 centimetres.

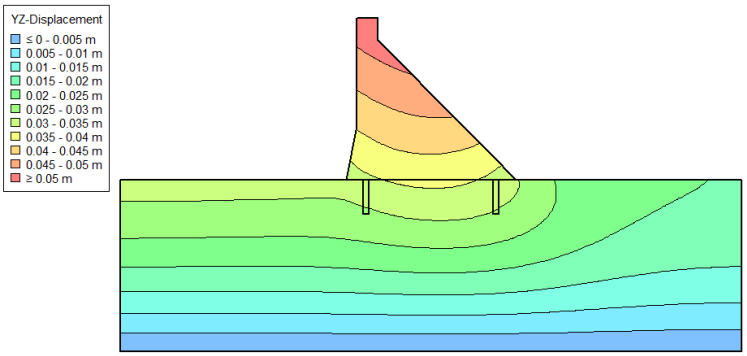

Figure 48. Displacement in the YZ-direction during NWL conditions

Shear stresses - NWL conditions

The shear stresses during NWL conditions can be seen in figure 49. The shear stress is overall 0-2 MPa in most of the structure. The highest shear stresses can be observed in the heel and the toe. The shear stresses reach up to 8 MPa at the heel, 6 MPa at the toe and around 4-6 MPa in the foundation underneath the heel and toe.

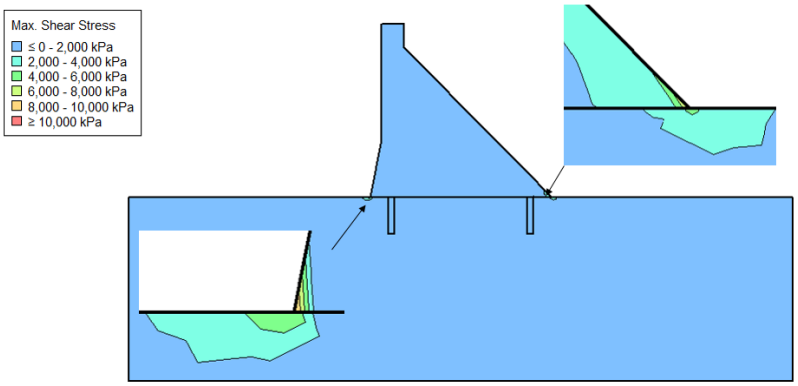

Figure 49. Shear stresses during NWL conditions

Stresses in Y-direction - NWL conditions

The stresses in the Y-direction during NWL conditions can be seen in figure 50. The stress in the Y-direction is around 0-2 MPa compression in most of the structure. The stresses in the Y-direction reach up to 4 MPa compression at the dam toe and -2 MPa tension in the dam heel. The foundation underneath the toe is subjected up to 5 MPa compression, while the foundation underneath the dam heel is subjected up to -4 MPa tension.

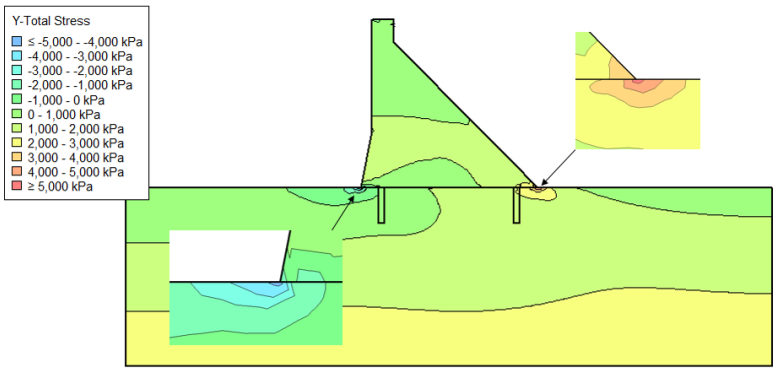

Figure 50. Stresses in the Y-direction during NWL conditions

Stresses in Z-direction - NWL conditions

The stresses in the Z-direction during NWL conditions can be seen in figure 51. The stress in the Z-direction is around 0-2 MPa compression in most of the structure. The stresses in the Z-direction reach up to 4 MPa compression at the dam toe and -6 MPa tension in the dam heel. The foundation is subjected to 4 MPa compression underneath the dam toe and up to -6 MPa tension underneath the dam heel.

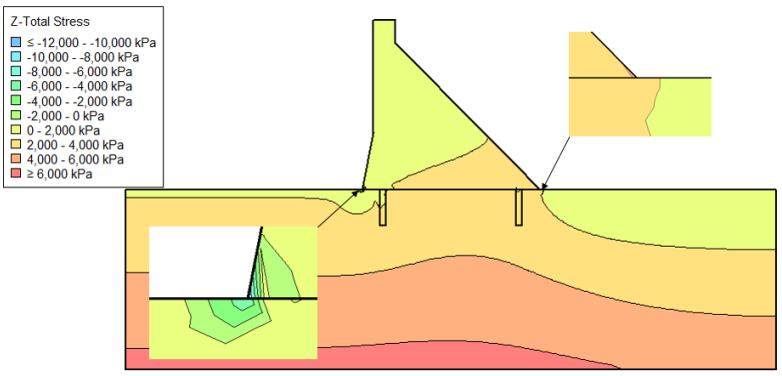

Figure 51. Stresses in the Z-direction during NWL conditions

Maximal stresses - NWL conditions

The maximal stresses during NWL conditions can be seen in figure 52. The maximal stresses reach up to 12 MPa compression in the dam toe and 10 MPa in the foundation underneath the dam toe. The maximal stress in the dam heel is around 2 MPa compression.

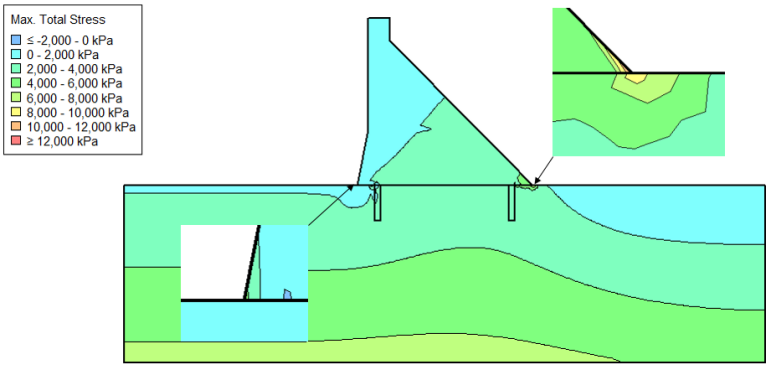

Figure 52. The maximal stresses during NWL conditions

Minimal stresses - NWL conditions

The minimal stresses during NWL conditions can be seen in figure 53. The minimal stress in the dam toe is -2 MPa tension. The minimal stress in the dam heel is around -14 MPa tension and the minimal stress in the foundation underneath the dam heel is around -10 MPa tension.

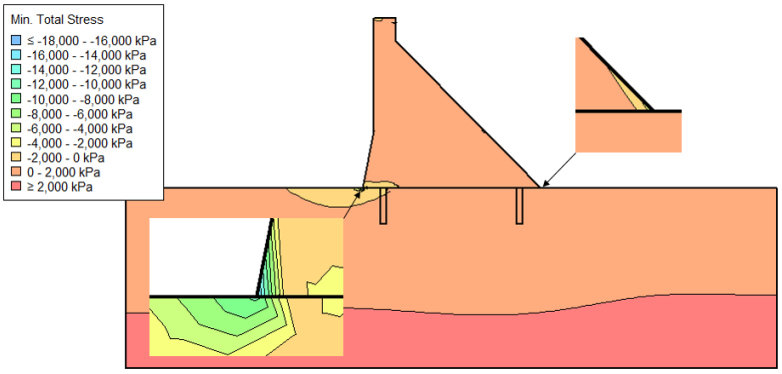

Figure 53. The minimal stresses during NWL conditions

Displacements – Deformed grid - CWL conditions

The deformed grid during CWL conditions can be seen in red in figure 54, where the displacements have been magnified with a factor of 350 to make the deformation noticeable. The dam seems to get tilted towards the downstream side and pressured down towards the foundation.

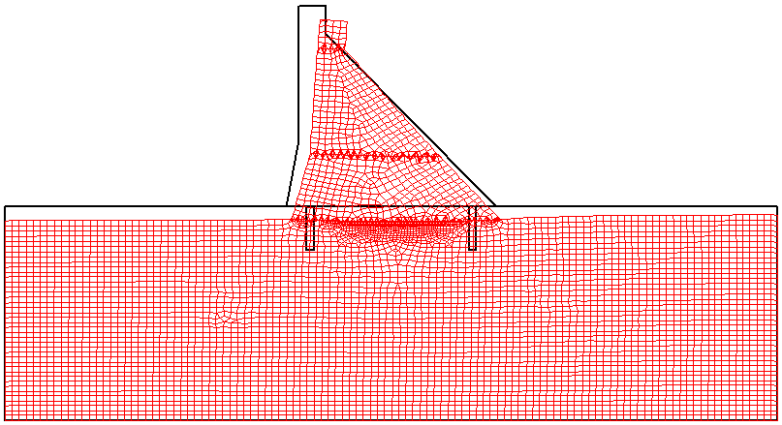

Figure 54. The deformed grid of the dam (magnified with a factor of 350) during CWL conditions

Displacements – Displacement vectors - CWL conditions

The displacement vectors during CWL conditions can be seen in red in figure 55. The vectors show towards which direction each point is going to be displaced. The displacement vectors at the top of the dam body are directed towards the dam toe while the vectors at the dam base are more vertical directed towards the foundation. This should imply that the top of the dam body wants to tilt to the downstream side while the base is pressured to the foundation.

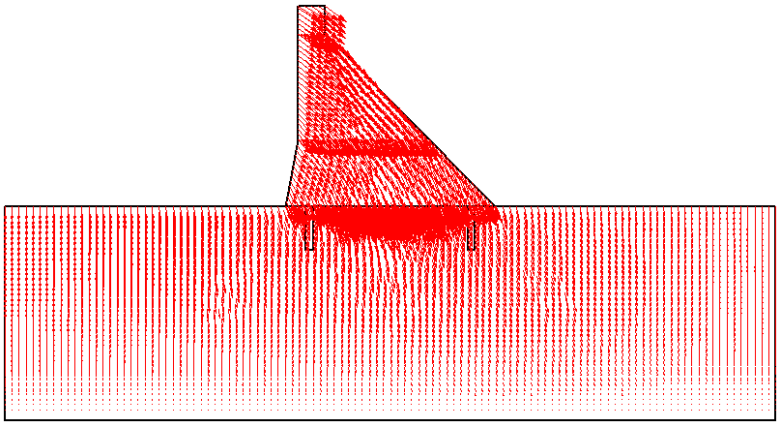

Figure 55. Displacement vectors during CWL conditions

Displacements in Y-direction - CWL conditions

Figure 56 shows the displacements in the Y-direction during CWL conditions. The colour scale on the left side in figure 56 shows what displacement each colour in the figure represents. The top of the structure is tilted 4,0 centimetres

to the downstream side. The foundation underneath the base of the dam is displaced around 1,0 centimetres to the downstream side.

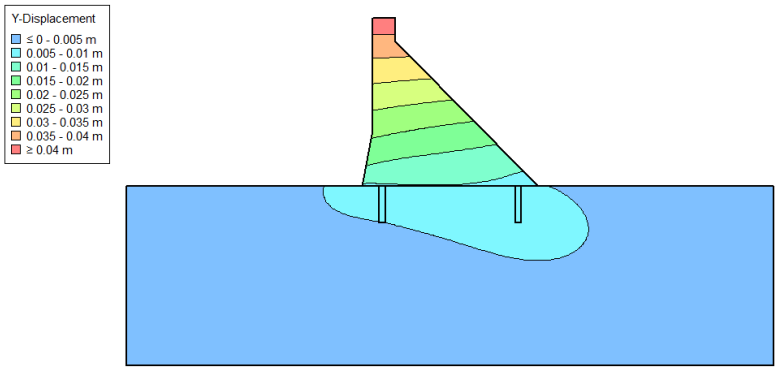

Figure 56. Displacement in the Y-direction during CWL conditions

Displacements in Z-direction - CWL conditions

Figure 57 shows the displacements in the Z-direction during CWL conditions. The colour scale on the left side in figurer 57 shows what displacement each colour in the figure represents. The displacement in the dark blue area at the top of the structure is 4,5 centimetres downwards. The foundation underneath the base of the dam is displaced circa 3,0 centimetres downwards.

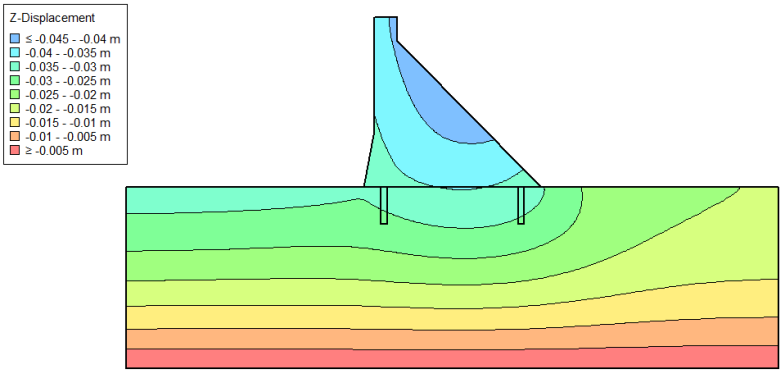

Figure 57. Displacement in the Z-direction during CWL conditions

Displacements in YZ-direction - CWL conditions

The displacement in the YZ-direction during CWL conditions can be seen in figure 58. The colour scale on the left side in figure 58 shows what displacement each colour in the figure represents. The displacement is around 6,0 centimetres in the YZ-direction at the top of the dam. At the foundation underneath the base of the dam the displacement in the YZ-direction is around 4,0 centimetres.

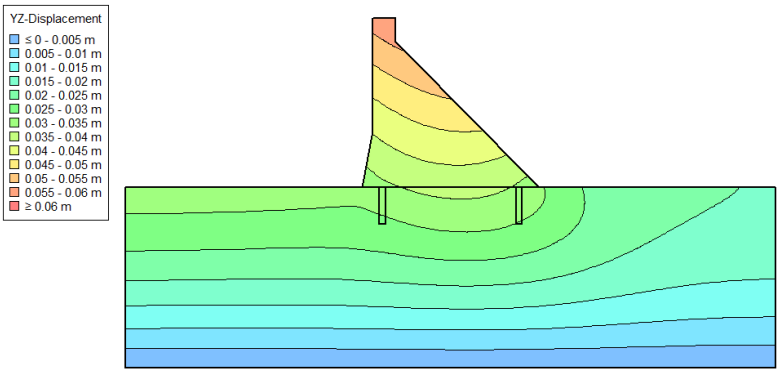

Figure 58. Displacement in the YZ-direction during CWL conditions

Shear stresses - CWL conditions

The shear stresses can be seen in figure 59. The shear stress is overall 0-2 MPa in most of the structure. The highest shear stresses can be observed in the heel and the toe. The shear stresses reach up to 10 MPa at the heel, 6 MPa at the toe and around 4-6 MPa in the foundation underneath the heel and toe.

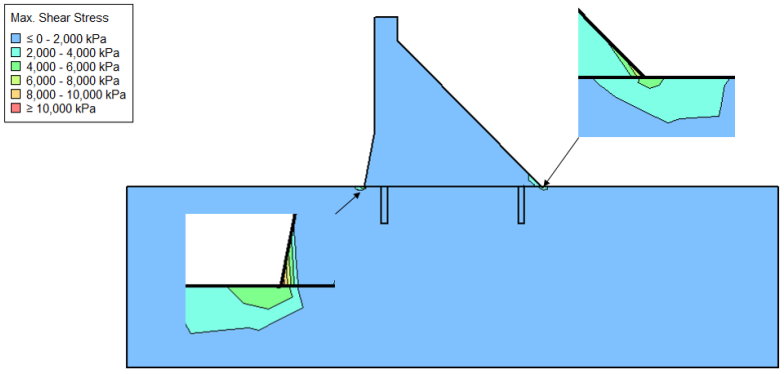

Figure 59. Shear stresses during CWL conditions

Stresses in Y-direction - CWL conditions

The stresses in the Y-direction during CWL conditions can be seen in figure 60. The stress in the Y-direction is around 0-2 MPa compression in most of the structure. The stresses in the Y-direction reach up to 4 MPa compression at the dam toe and -2 MPa tension in the dam heel. The foundation underneath the toe is subjected up to 4 MPa compression, while the foundation underneath the dam heel is subjected up to -6 MPa tension.

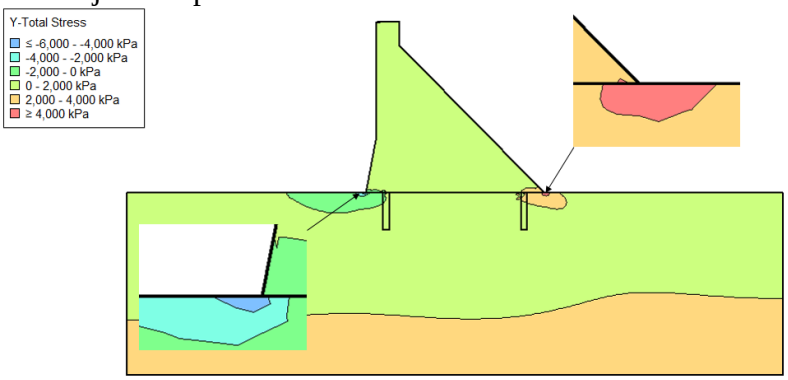

Figure 60. Stresses in the Y-direction during CWL conditions

Stresses in Z-direction - CWL conditions

The stresses in the Z-direction during CWL conditions can be seen in figure 61. The stress in the Z-direction is around 0-2 MPa compression in most of the structure. The stresses in the Z-direction reach up to 6 MPa compression at the dam toe and -8 MPa tension in the dam heel. The foundation is subjected to 4MPa compression underneath the dam toe and up to -6 MPa tension underneath the dam heel.

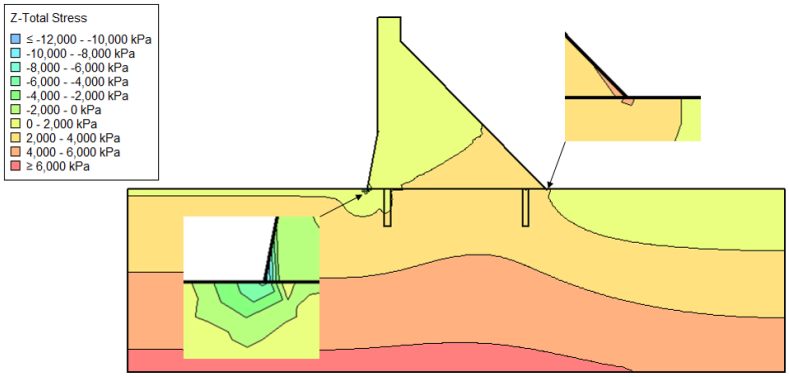

Figure 61. Stresses in the Z-direction during CWL conditions

Maximal stresses - CWL conditions

The maximal stresses during CWL conditions can be seen in figure 62. The maximal stresses reach up to 12 MPa compression in the dam toe and 10 MPa the foundation underneath the dam toe. The maximal stress in the dam heel is around 2-4 MPa compression.

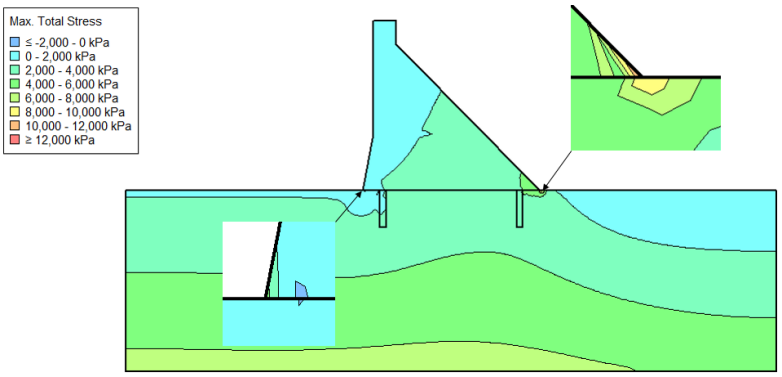

Figure 62. The maximal stresses during CWL conditions

Minimal stresses - CWL conditions

The minimal stresses during CWL conditions can be seen in figure 63. The minimal stress in the dam toe is -2 MPa tension. The minimal stress in the dam heel is around -16 MPa tension and the minimal stress in the foundation underneath the dam heel is around -10 MPa.

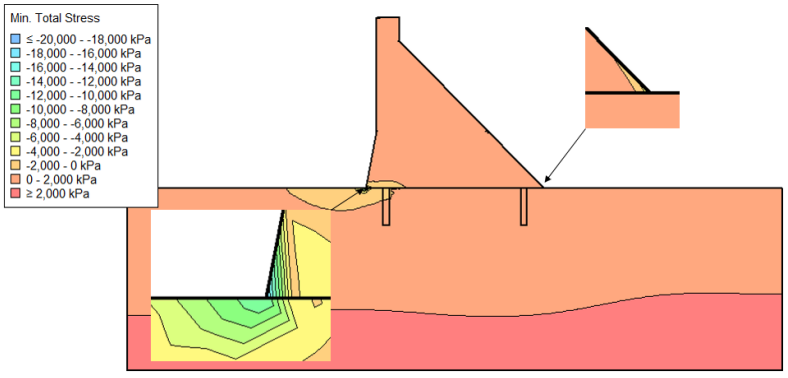

Figure 63. The minimal stresses during CWL conditions

11.5.2. Discussion

Displacement analysis

The results from the displacement analysis in SIGMA/W show that the dam is going to tilt slightly towards the downstream side and that there will be some settlement of the structure. This behaviour seems reasonable when considering the loads that are acting on the structure. The horizontal hydrostatic pressure will try to overturn the dam while the self-weight of the dam will push the structure down towards the foundation.

The displacements are in the magnitude of a couple of centimetres. The values might seem large, but when the displacements are put in proportion to the large dam dimensions they are not very significant. The dam is over 180 meters tall and 150 meters wide. A displacement of a couple centimetres corresponds to a strain in the magnitude of one tenth of a per mille with the current dam dimensions.

A comparison between the displacement vectors during NWL conditions (figure 45) and CWL conditions (figure 55) reveals no significant difference in the behaviour of the structure. However, a comparison of the deformed grid in figure 44 and figure 54 shows that the dam is more tilted towards the downstream side during CWL conditions than during NWL conditions. Figure 46 and figure 56 shows that the displacement in Y-direction at the top of the dam is slightly higher during CWL conditions (4,0 centimetres) than during NWL conditions (3,2 centimetres). But the displacement in the Y-direction below the base of the dam is very similar for both cases (around 1,0 centimetres). No significant difference can be observed in the displacement in the Z-direction between the results from the NWL case and the CWL case (figure 47 and figure 57). The displacements in the Z-direction at the top of the dam body measure up to circa 4,0 centimetres while the displacement in the foundation underneath the dam base is circa 3,0 centimetres. A small difference in the displacement in the YZ-direction can be observed in the results from the different upstream water levels. The displacement in the YZ-direction at the top of the structure is 6,0 centimetres during CWL conditions and 5,0 centimetres during NWL conditions, but otherwise the results (figure 48 and figure 58) are very similar. It is reasonable that the displacements are slightly higher during CWL conditions than during NWL conditions due to the higher hydrostatic loading during CWL conditions.

Stress analysis

Concrete can withstand between 12-50MPa compression depending on the concrete class (Isaksson & Mårtensson 2010). But concrete has a low tensile capacity and tension should be avoided because it will lead to cracks. The material properties for limestone can vary a lot depending on the sample. The tensile strength for limestone can range from 5-25 MPa and the compressive strength can be 13,8-255 MPa (Matweb, n.d). The results from the stress analysis in SIGMA/W show that the most of the dam body is subjected to uniform stresses with acceptable values, except in the heel and the toe where there are stress concentrations.

The distribution of stresses is very similar during both NWL conditions and CWL conditions. The only significant difference is that the stresses during CWL conditions are around 2 MPa higher than during NWL conditions in the areas with peak values (the dam heel and dam toe). This is reasonable as the hydrostatic loading is higher during CWL conditions than during NWL conditions.

The shear stress is 0 MPa in most of the dam body (figure 49 and figure 59). The shear stress in the heel reaches up to 8 MPa during NWL conditions and 10 MPa during CWL conditions. The toe is subjected to 6 MPa shear stress during both NWL and CWL conditions. The compressive stress in the dam is in general around 0-4 MPa in most of the dam structure during both cases (figure 52 and figure 62). The peak compressive stress values can be observed in the dam toe where the compression is 10 MPa during NWL conditions and 12 MPa during CWL conditions. The tensile stress is 0 MPa in most of the dam body in both cases, except in the dam heel where the tension is -14 MPa during NWL conditions and -16 MPa during CWL conditions (figure 53 and figure 63). The highest compressive stress in the foundation is 10 MPa (figure 62) and occurs under the toe. The highest tensile stress in the foundation is -10 MPa and it can be observed underneath the dam heel (figure 63).

The high stress values in the heel and toe of the dam are most likely caused by stress singularities. Stress singularities occur in sharp corners of a FE-model and result in unreasonably high stress values that grow to infinity unless a stress limit is defined for the materials in the FE-model (Sönnerlind, 2015). Further investigations are necessary to determine how the peak stresses will

affect the materials. The limestone can resist the peak stresses if the foundation is of sufficient strength. The concrete can endure the peak compressive stresses in the dam toe, but the high tensile stresses in the dam heel will lead to a tensile failure. In reality this will lead to cracks in the concrete in the sharp corner of the dam heel, and the stresses will be redistributed. The effect of this can be comparable to changing the fillet radius of the sharp corners and it will not lead to problems to the rest of the structure, unless the loadings are cyclic which can cause fatigue (Sönnerlind, 2015).

12. Conclusions

Even though the design mainly follows values and expressions from Chinese Standards, these are in turn based on international regulations like the Eurocodes and the work produced by the USBR.

The results obtained in this preliminary design ensure that the non-overflow section is safe against compressive stress and overturning. However, it is recommended that the self-weight of the dam is slightly increased so that the structure is sufficiently safe against sliding. Moreover, even though the analytical calculations did not show it, the FEM modelling indicates the risk for tensile failure is high in the dam heel. Therefore, reinforcements in the dam heel should be considered to avoid seepage problems. Furthermore, a stilling basing must be added to the design to prevent erosion downstream.

References

Alchetron. 2018. *Sanmenxia dam* [picture]. https://alchetron.com/Sanmenxia-Dam#- (2019-10-14)

Allan, M.L. and Philippacopoulos. 1999. *Properties and Performance of Cement-based Grout for Geothermal Heat Pump Applications*. Washington, D.C., USA: United States Department of Energy

Ancient Origins. 2013. *The Dujiangyan irrigation system* [picture]. https://www.ancient-origins.net/news-history-archaeology-ancient-technology/legacy-dujiangyan-china-s-ancient-irrigation-system (2019-10-14)

Chen, S. H., & Chen, M. L. 2015. *Hydraulic Structures*. Berlin, Germany: Springer Verlag GmbH.

China Electricity Council. 2013. *GB50199-2013 - Unified Design Standard for Reliability of Hydraulic Engineering Structures*. Beijing, P.R. China: Ministry of Housing and Urban-Rural Development

Chinese National Committee on Large Dams (Chincold). n.d. *Longtan Hydropower Project*. Beijing, P.R. China: Chinese National Committee on Large Dams

Chinese National Committee on Large Dams (Chincold). n.d. Non-overflow section of the Longtan dam [picture]. *Longtan Hydropower Project*. Beijing, P.R. China: Chinese National Committee on Large Dams

Chinese National Committee on Large Dams (Chincold). n.d. Overflow section of the Longtan dam [picture]. *Longtan Hydropower Project*. Beijing, P.R. China: Chinese National Committee on Large Dams

Cleveland, C.J. and Morris, C. 2014. *Handbook of Energy – Volume II: Chronologies, Top Ten Lists, and Word Clouds*. Oxford, United Kingdom: Elsevier Inc.

Dams and Spillways Sectional Committee. 2010. *IS 7365:2010 - Criteria for Hydraulic Design of Bucket Type Energy Dissipators*. 2nd revision. New Delhi, India: Bureau of Indian Standards

Engineering ToolBox. 2008a. *Poisson's ratio*. https://www.engineeringtoolbox.com/poissons-ratio-d_1224.html (2019-10-18)

Engineering ToolBox. 2008b. *Concrete – Properties*. https://www.engineeringtoolbox.com/concrete-properties-d_1223.html (2019-10-18)

Fine. n.d. *Unit Weight of Rocks*. https://www.finesoftware.eu/help/geo5/en/unit-weight-of-rocks-01/ (2019-10-18)

Garg, S.K. 2006. *Irrigation Engineering and Hydraulic Structures*. Delhi, India: Khanna Publishers

GEOSLOPE. n.da *GEOSLOPE>About*. https://www.geoslope.com/about (2019-10-04)

GEOSLOPE. n.db *GeoStudio>Products*. https://www.geoslope.com/products/geostudio (2019-10-04)

GEO-SLOPE International, Ltd. 2012. *Seepage Modelling with SEEP/W*. Calgary, Canada: GEO-SLOPE International, Ltd.

GEO-SLOPE International, Ltd. 2013. *Stress-Deformation Modelling with SIGMA/W*. Calgary, Canada: GEO-SLOPE International, Ltd.

Graham, A. 1997. *Table of Modulus of Elasticity of Rock*. Durham University Community. http://community.dur.ac.uk/~des0www4/cal/dams/geol/geolf17.htm (2019-10-18)

Hamill, L. 2011. *Understanding Hydraulics*. 3rd edition. Basingstoke, United Kingdom: Palgrave Macmillan

Huang, H and Yan, Z. 2009. Present situation and future prospect of hydropower in China. *Renewable and Sustainable Energy Reviews* 13 (6-7) 1652-1656

International Hydropower Association (IHA). 2019. *2019 hydropower status report – sector trends and insights*. London, United Kingdom: International Hydropower Association Limited

International Rivers. n.d. *Environmental Impacts of Dams*. https://www.internationalrivers.org/environmental-impacts-of-dams (2019-12-02)

International Water Power & Dam Construction. 2014. RCC Dams: Simplicity is the key to success. International Water Power & Dam Construction. April 23rd. https://www.waterpowermagazine.com/features/featurercc-dams-simplicity-is-the-key-to-success-4219225/ (2019-09-24)

Isaksson, T and Mårtensson, A. 2010. *Byggkonstruktion Regel- och formelsamling*. 2nd edition. Lund, Sweden: Studentlitteratur AB

Johansson, B and Sellberg, B. 2006. *Dams under Debate*. Stockholm, Sweden: Swedish Research Council Formas

Lai, H and Warner, M. 2016. *Managing China's Energy Sector – Between the market and the state*. New York, USA: Taylor & Francis

Le Grand Portage. 2009. The Three Gorges dam [picture]. https://commons.wikimedia.org/wiki/File:Three_Gorges_Dam,_Yangtze_River,_China.jpg (2019-10-14)

Lerer, L.B and Scudder, T. 1999. Health impacts of large dams. *Environmental Impact Assessment Review* 19 (2) 113-123

Li, X.Z., Chen, Z.J., Fan, X.C. and Cheng Z.J. 2018. Hydropower development situation and prospects in China. *Renewable and Sustainable Energy Reviews* 82 (1) 232-239

Linsley, R.K., Franzini, J.B., Freyberg, D.L. and Tchobanoglous G. 1992. *Water-Resources Engineering*. Singapore: McGraw-Hill Inc.

Liu, J., Zang, C., Tian, S., Liu, J., Yang, H., Jia, S., You, S., Liu, B and Zhang, M. 2013. Water conservancy projects in China: Achievements, challenges and way forward. *Global Environmental Change* 23 (3) 633-643

Malcolm Dunstan and Associates (MD & a). n.da. *RCC Dams – Longtan Dam*. Malcolm Dunstan and Associates. http://www.rccdams.co.uk/dams/longtan/ (2019-09-10)

Malcolm Dunstan and Associates. n.da. *The Longtan dam during operation* [picture]. http://www.rccdams.co.uk/dams/longtan/ (2019-10-14)

Malcolm Dunstan and Associates. n.db. The Shapai dam during construction [picture]. http://www.rccdams.co.uk/dams/shapai/ (2019-10-14)

Mason, P.J. 1993. Practical guidelines for the design of flip-buckets and plunge pools. *Water Power and Dam Construction* 45 (9) 40-45

MatWeb. n.d. *Limestone*. http://www.matweb.com/search/datasheet.aspx?matguid=87597d62662c46a7a308b11e16c563c6&ckck=1 (2019-10-23)

Mesic, A., Beal, D and Heywood, R. 1994. *Measuring Water Permeability of Concrete and its Applications*. Brisbane, Australia: Queensland University of Technology

Ministry of Water Resources. 2005. *SL319-2005 - Design Specification for Concrete Gravity Dams*. Beijing, P.R. China: China Water Power Press

Natural Resources Conservation Service (NRCS). 2004. *National Engineering Handbook: Part 630—Hydrology*. Washington, D.C., USA: United States Department of Agriculture

Novak, P. Moffat, A.I.B. Nalluri, C and Naranyan, R. 2007. *Hydraulic Structures*. 4th edition. New York, USA: Prentice Hall

Otte. 2018. *GeoStudio Products*. http://ottegroup.com/geotechnical-engineering/geostudio/products/ (2019-10-04)

Ottosen, N.S and Petersson, H. 1992. *Introduction to the finite element method*. Essex, United Kingdom: Pearson Education Limited

Portland Cement Association. n.d. *Roller-Compacted Concrete (RCC)*. America's Cement Manufacturers. https://www.cement.org/cement-concrete-applications/paving/roller-compacted-concrete-(rcc) (2019-09-24)

Punmia, B.C. and Pande, B.B.L. 1992. *Irrigation and Water Power Engineering*. 12th edition. New-Delhi, India: Laxmi Publications Ltd.

Qingchung, S and Feng, X. n.d. *Several Main Technical Issues in the Design of High RCC Gravity Dam of Longtan Hydropower Station.* Changsha, P.R. China: Powerchina Zhongnan Engineering Corporation Limited

Rajan, B.H. and Shivashankara Rao, K.N. 1980. Design of trajectory buckets. *Irrigation and Power* 37 (1) 63-76

Scientific American. 2018. *The Downside of Dams: Is the Environmental Price of Hydroelectric Power Too High?* https://www.scientificamerican.com/article/how-do-dams-hurt-rivers/ (2019-12-02)

Shen, F. 2018. China Steps Up Its Push Into Clean Energy. *Bloomberg*. September 26th. https://www.bloomberg.com/news/articles/2018-09-26/china-sets-out-new-clean-energy-goals-penalties-in-revised-plan (2019-09-18)

Shurong, F and Feng, X. n.d. *The design of Longtan Roller Compacted Concrete gravity dam*. Changsha, P.R. China: Mid-south Institute for Hydropower Projects

SoilSensor. n.d. *Soil Matric Potential*. https://soilsensor.com/articles/soil-matric-potential/ (2019-10-21)

State Economy and Trade Commission of the People's Republic of China. 1999. *DL5108-1999 - Design Specification for Concrete Gravity Dams*. Beijing, P.R. China: China Electric Power Press

Sönnerlind, H. 2015. *Singularities in Finite Element Models: Dealing with Red Spots*. COMSOL. https://www.comsol.com/blogs/singularities-in-finite-element-models-dealing-with-red-spots/ (2019-10-04)

UNESCO. n.d. *Mount Qingcheng and the Dujiangyang Irrigation System*. UNESCO. https://whc.unesco.org/en/list/1001/ (2019-09-16)

United States Bureau of Reclamation. 1987. *Design of Small Dams*. Washington, D.C., USA: US Department of the Interior, Bureau of Reclamation

United States Department of the Interior. 2014. *Design Standards No.14 – Appurtenant Structures of Dams (Spillways and Outlet Works) Design Standard – Chapter 3: General Spillway Design Considerations*. Washington D.C., USA: United States Bureau of Reclamation

U.S. Army Corps of Engineers. 2009. The Willow Creek dam [picture]. https://en.wikipedia.org/wiki/Willow_Creek_Dam_(Oregon)#/media/File:Willowcr.jpg (2019-10-14)

U.S. Army Waterways Experimental Station. 1959. Crest profile of an ogee spillway [picture]. *Hydraulic Design Criteria*. Washington D.C., USA: USA Department of the Army

Wang, B., Zhou, J and Chen, G. n.d. *Special design requirements for high RCC gravity dam*. Beijing, P.R. China: China Hydropower Consulting Group Co.

Wang, P., Dong, S and Lassoie J.P. 2014. *Large Dams in China: An Overview of History, Distribution, and Case Studies*. Dordrecht, the Netherlands: Springer

Warren, T. 2015. World class achievements as dam reach new heights. *International Water Power & Dam Construction*. 11 February. https://www.waterpowermagazine.com/features/featureworld-class-achievements-as-dams-reach-new-heights-4509863/ (2019-09-10)

Zhang, D., Wang, J., Lin, Y., Si, Y., Huang, C., Yang, J., Huang, B and Li, W. 2017. Present situation and future prospect of renewable energy in China. *Renewable and Sustainable Energy Reviews* 76 865-871

Zhang, L. 1999. *Social Impacts of Dams: The China Case*. Beijing, P.R. China: Chinese Academy of Agricultural Sciences

Zhang, Y., Zhang, F., Wu, S., Yuan, B., Feng, J., Fu, G., Li, N and Chen L. 2019. *Non-Fossil Energy Development In China – Goals and Challenges*. London, United Kingdom: Elsevier Inc.